ISSN 2543-9901

JOURNAL OF CASTING & MATERIALS ENGINEERING

QUARTERLY
Vol. 7 No. 4/2023

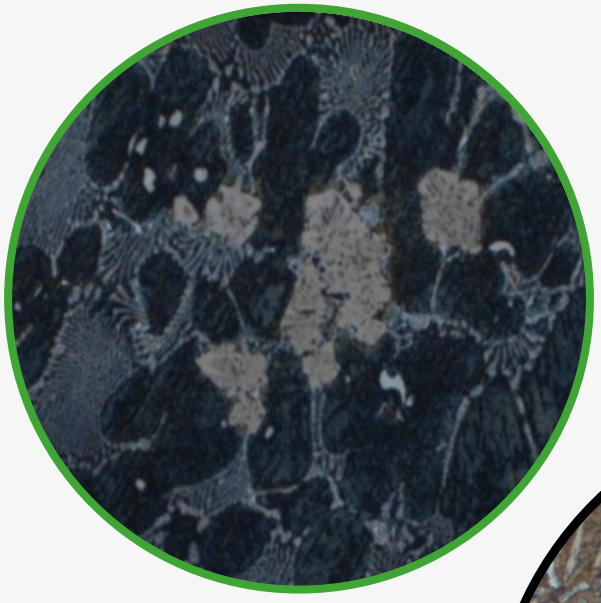

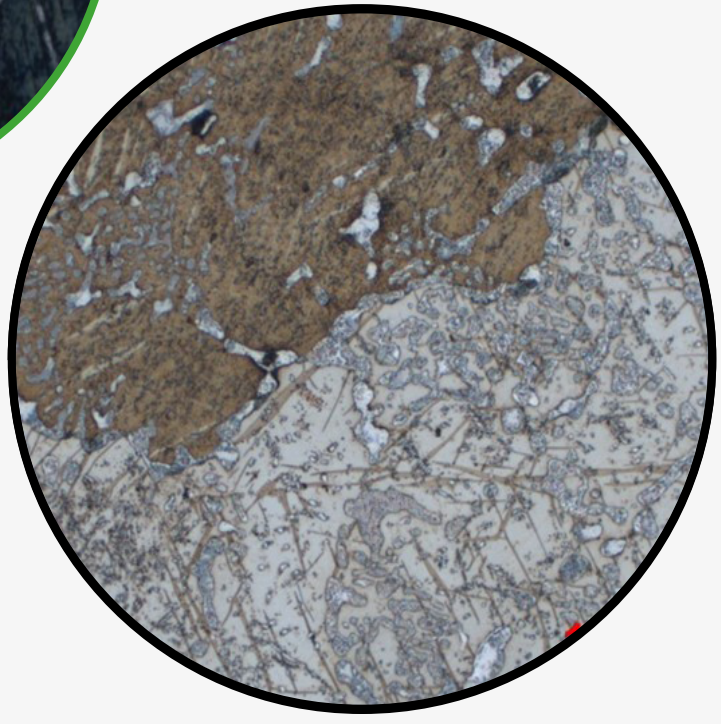

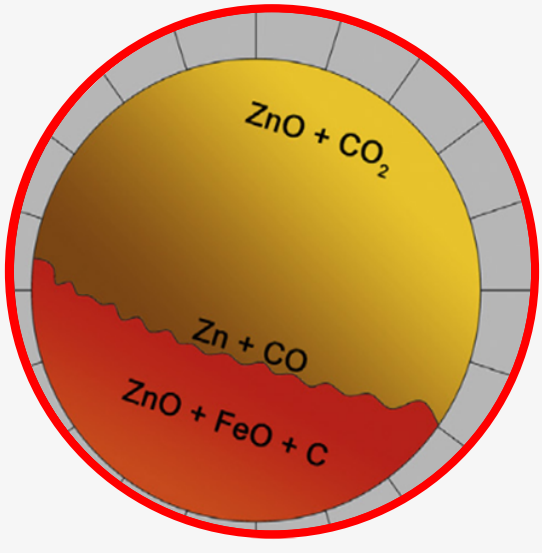

JCME

AGH UNIVERSITY OF KRAKOW
FACULTY OF FOUNDRY ENGINEERING

AGH UNIVERSITY PRESS
KRAKOW 2023

The articles published in the Journal of Casting & Materials Engineering have been given a favorable opinion by the rewievers designated by the Editorial Board.

www:
https://journals.agh.edu.pl/jcme/

AGH UNIVERSITY PRESS KRAKOW 2023

Wydawnictwa AGH (AGH University Press)
al. A. Mickiewicza 30, 30-059 Kraków
tel. 12 617 32 28, 12 638 40 38
e-mail: redakcja@wydawnictwoagh.pl
http://www.wydawnictwa.agh.edu.pl

Contents

Journal of Casting & Materials Engineering Vol. 7 No. 4 (2023) 41–48
https://doi.org/10.7494/jcme.2023.7.4.41

Polylactide Used as Filament in 3D Printing – Part 2: TG-DTG, DSC and DRIFT Investigations

Beata Grabowska*, Mateusz Skowron, Karolina Kaczmarska

AGH University of Krakow, Faculty of Foundry Engineering, Reymonta St. 23, 30-059 Krakow, Poland
e-mail: beata.grabowska@agh.edu.pl

Received: 11 July 2022/Accepted: 23 September 2023/Published online: 1 October 2023
This article is published with open access at AGH University of Science and Technology Journals

Abstract

In this second part of the article, we delve deeper into the research area initiated in the first part, focusing on the critical exploration of polylactide (PLA) modification to enhance thermal and mechanical properties in PLA-based materials, building upon the insights obtained from comprehensive structural and thermal analyses utilizing analytical methods such as infrared spectroscopy (FTIR), diffuse reflectance infrared spectroscopy (DRIFT), and thermoanalytical research (DRIFT, TG-DTG). A series of structural and thermal analysis research (TG-DTG, DSC, DRIFT) were performed for samples of polylactide (PLA), which is commonly used in additive technologies as a structural material. In total, four materials were considered, including two containing dyes with different colors, a material made of PLA recyclate and a graphene-modified PLA material. It was noted that PLA material reinforced with graphene phase (GRAFYLON®) retains the best thermal properties (TG-DTG), which results in its wider potential for processing, including further modification and usability in manufacturing vehicle structural elements. Recycled PLA material (ALFA+W) was characterized by a higher melting point (T_p) by more than 20°C than other samples (DSC analysis), so it can be more useful in the production of structural elements operating and used at elevated temperatures.

Keywords:

polylactide, graphene, recycling, 3D printing technology, thermal degradation, TG-DTG, DSC, DRIFT

1. INTRODUCTION

3D printing technology is widely used in the design and manufacturing process of vehicle structural components. Production changes that are currently being implemented are mainly related to the diversification of manufacturing methods and techniques, while reducing waste and sourcing recycled materials. Between 2018 and 2021, approx. 20% of Gartner's Global Top 100 companies have used additive manufacturing methods to produce customized products. It Is predicted that by 2025, expenditure on 3D printing technologies is expected to grow at a compound annual growth rate of 15.5%. With this growth, the market is expected to double up in the value over the next four years. It is also projected that there will be a 100% increase in the use of 3D printing for the automotive and aerospace industries during this time [1, 2].

The dynamic development of the 3D printing industry has led manufacturers of materials used in 3D printing to introduce significant improvements in the technologies applied. Material modifications are being carried out in this area, e.g. composites of polymeric materials are being produced, which are largely based on the addition of recyclates. Companies invest substantial funds in R&D departments that develop innovative materials used in additive manufacturing. A trend that is currently underway is based on the production of biodegradable materials derived from natural sources, as well as those from recyclable waste) [3].

This research represents the next stage of work on the verification of polylactide-containing materials for their ultimate use as a base material in the production of new filament. Nowadays, composites and plastics containing poly(lactic acid) called polylactide (PLA) are widely used engineering materials, also in the automotive industry) [4–6]. Therefore it is important to recognize the physicochemical properties of such commercial materials in detail, also in view of undertaking our own research on PLA modification or creating new composite materials with its participation. In the first part of the publication, a comprehensive thermoanalytical analysis (FTIR, DRIFT, TG-DTG) was performed. It allowed us to determine the temperature range in which commercially available polylactide does not undergo thermal degradation, but it only takes reversible transformations so it does not lose its functional properties. Based on the obtained results in our first part of article [7], PLA was found to be thermally stable in the temperature range of 25–300°C. Thus, the operating temperature of a typical 3D printer, in which the processing of polylactide occurs, is not exceeded (extrusion temperature is not exceeded) [7, 8].

PLA is a biodegradable polyester and is most often made from renewable raw materials. The properties of PLA depends on the constituent isomers, processing temperature, annealing time and molecular weight. PLA homopolymers have a very narrow processing window. A method to improve processing properties involves: lowering the melting temperature by adding randomly small amounts of enantiomers of lactide with opposite configuration into the polymer, e.g. adding D-lactide to L-lactide to obtain PDLLA. Unfortunately, as a consequence, lowering the temperature leads to a significant decrease in the strength of PLA products. High molecular weight poly(lactic acid) is a colorless, glossy, rigid thermoplastic polymer with similar properties to polystyrene. It is not soluble in water, but it is in dichloromethane and dimethylformamide [9–11].

PLA is increasingly being used in the automotive industry, but it has not been easy due to the increased cost of manufacturing. Ford and Toyota were the first automotive corporations to use PLA in their vehicles and mass production with polylactide based components was initiated by the Japanese brand Mazda. Polylactide is used in the production of seat upholstery, car mats, headliner surfaces, dashboards. PLA is UV resistant which makes it a good replacement for common plastics such as polypropylene (PP), poly(ethylene terephthalate) (PET), or acrylonitrile-butadiene styrene terpolymer (ABS). An additional advantage is that it is eco-friendly [12–14].

PLA filament is not very sensitive to temperature changes and has excellent surface quality. It works well for printing complex structural components. The printing process can be carried out in a low temperature range but PLA is more brittle than ABS and less flexible compared to polymer fibres. On the other hand, it is susceptible to painting with primer and to bonding by gluing with a wide range of adhesives, including cyanoacrylates, yet care must be taken during the hot bonding process to avoid the melting of the material [13, 14]. Table 1 summarizes the general characteristics of PLA.

Table 1
Characteristics of the basic PLA filament used in 3D printing [15]

Density [kg/m^3]	1200–1240
Glass transition temp. [°C]	55.0–60.0
Coefficient of linear thermal expansion [1/°C]	8.5×10^{-5}
Process shrinkage [%]	0.3–3.0
Tensile stress [MPa]	25.0–41.0
Young's modulus [GPa]	3.5–3.6
Shore hardness [ShD]	85.0–97.0
Min. continuous operating temperature [°C]	50.0–87.0
Printing temperature [°C]	190–230
Automotive application	instrument panels, dashboards, decorative for interior, headliner

2. METHODOLOGY

2.1. Materials

The following polylactide filament samples were used in this study:

- PLA1 – pure polylactide based filament, color: transparent, density: 1.24 g/cm^3, diameter: 1.75 mm (manufacturer: AGH);
- PLA7 – commercial PLA filament, color: blue, density: 1.24 g/cm^3, diameter: 1.75 mm (manufacturer: Fiberlogy);
- ALFA+W – commercial polymeric filament based on PLA, color: silver, density: 1.30 g/cm^3, filament diameter: 1.75 mm, base material is polylactide produced from recycled materials containing above 80% of recyclate (manufacturer: FILOALFA);
- GRAFYLON® – commercial polymeric filament based on PLA matrix (composite of graphene and PLA), color: graphite, density: 1.23 g/cm^3, diameter: 1.75 mm; filament is reinforced with graphene phase in the form of pure graphene nano-flakes (manufacturer: FILOALFA and Directa Plus).

2.2. Thermal analysis by TG-DTG-DSC

TG-DTG test were performed in accordance with PN-EN ISO 11358-1:2014-09 [16] using TGA/SDTA 851e thermogravimeter from Mettler-Toledo. The following parameters were used: temperature range: 25–900°C, heating rate: 10°C/min. The analysis was performed in an atmosphere of synthetic oxygen of 99.9992% purity. The gas flow through the furnace was set on: 60 ml/min. Aluminum oxide (Al_2O_3) crucible pots were used for this study. The temperature value of the center point of the T_c distribution was take as the temperature value of the maximum peak of the DTG curve. The initial weights of the samples were as follows: PLA1 – 14.164 mg; PLA7 – 14.594 mg; ALFA+W – 14.443 mg; GRAFYLON® – 14.986 mg.

DSC analysis was performed according to PN-EN ISO 11357-1:2016-11 [17] and PN-EN ISO 11357-2:2020-09 [18]. The temperature and enthalpy of melting and crystallization were also determined using a Mettler-Toledo DSC 822e differential scanning calorimeter. The test was performed according to the test standard PN-EN ISO 11357-3:2018-06 [19]. The following test parameters were used: temperature range: 0–180°C. For the ALFA+W samples, a higher temperature range 0–210°C was used. Analysis carried out up to the final measurement temperature of 180°C did not allow the extrapolated value of the melting end to be determined. Heating and cooling rate used: 10°C/min, duration of isometric segments: 5 min. A synthetic oxygen atmosphere of 99.9992% purity with 60 ml/min flow rate was used, an Al – pure aluminum crucible 40 µl with perforated lid. Initial samples massed: PLA1 – 9.04 mg, PLA7 – 9.03 mg, ALFA+W – 9.44 mg, GRAFYLON® – 8.75 mg.

2.3. Thermal analysis by diffuse reflectance technique (DRIFT)

DRIFT investigations were performed using a Bruker "Vertex 70V" vacuum spectrometer operating in the mid- and far-infrared in the wavenumber range of 8000–370 cm^{-1} and

700–30 cm^{-1}. Spectra were recorded in the temperature range 20–500°C and wave number range 4000–500 cm^{-1} with a preset resolution of 4 cm^{-1}. Interferograms consisted of 64 scans, which were averaged into one spectrum.

Test sample preparation involved grinding the test materials in an agate mortar (200 mg KBr and 2 mg polymer plastic samples). The powdered materials were directly placed in the measuring crucible. The ceramic crucible was placed inside the dome in the spectrometer. The windows of the dome were made of zinc selenium ZnSe. The spectrometer operated in coupling with "Opus Operator" software, which recorded the received spectra from the analytical instrument. Measurements were made at a rate of 10°C/min.

3. RESULTS AND DISCUSSION

3.1. Thermal analysis

Figures 1a–d show the TG-DTG results for polylactide samples. Thermal decomposition of both PLA1 sample (Fig. 1a), PLA7 sample (Fig. 1b), ALFA+W (Fig. 1c) and GRAFYLON® (Fig. 1d) started at the same moment (after reaching the temperature of 300°C).

Thermal degradation of the PLA1 sample occurred in the temperature range 353–466°C, and the total mass loss was 99.9%, which indicated its virtually complete degradation. For the PLA7 material, the degradation pattern was similar to that recorded for PLA1. However, in the case of PLA7, the degradation took longer, up to the temperature of about 466°C, the sample actually degraded completely. ALFA+W sample made of recycled material showed the highest thermal stability, the first weight loss was only 84.1% in the temperature range of 25–351°C. On the other hand, the sample modified with graphene nanoplatelets showed higher thermal stability than the polylactide PLA1 and PLA7 samples.

In Figures 2–5 the recorded DSC curves for the considered filament samples are shown.

Based on the analysis of the DSC curves, it can be concluded that the polylactide has a relatively low glass transition temperature (T_g) oscillating at 60°C. Material recycling and reinforcement has no significant effect on T_g value. Highest T_g value was determined for PLA7 polymer (T_g = 60.16°C). On the other hand, the filament ALFA+W produced from the recyclate had the lowest T_g value (T_g = 60.07°C). The melting point (T_p) of the polymeric materials which indicates the moment when the material undergoes the complete transition to the liquid state was also determined. Highest value of T_p was obtained for ALFA+W polymeric filament (T_p = 175.89°C). It can be caused by reuse of recyclate already used, which were remelted and regranulated and additionally could consist of modified materials. Rest of the materials had similar melting point valued in the range of 150–155°C. The results of the glass transition temperature and melting point temperature for PLA samples are shown in Table 2.

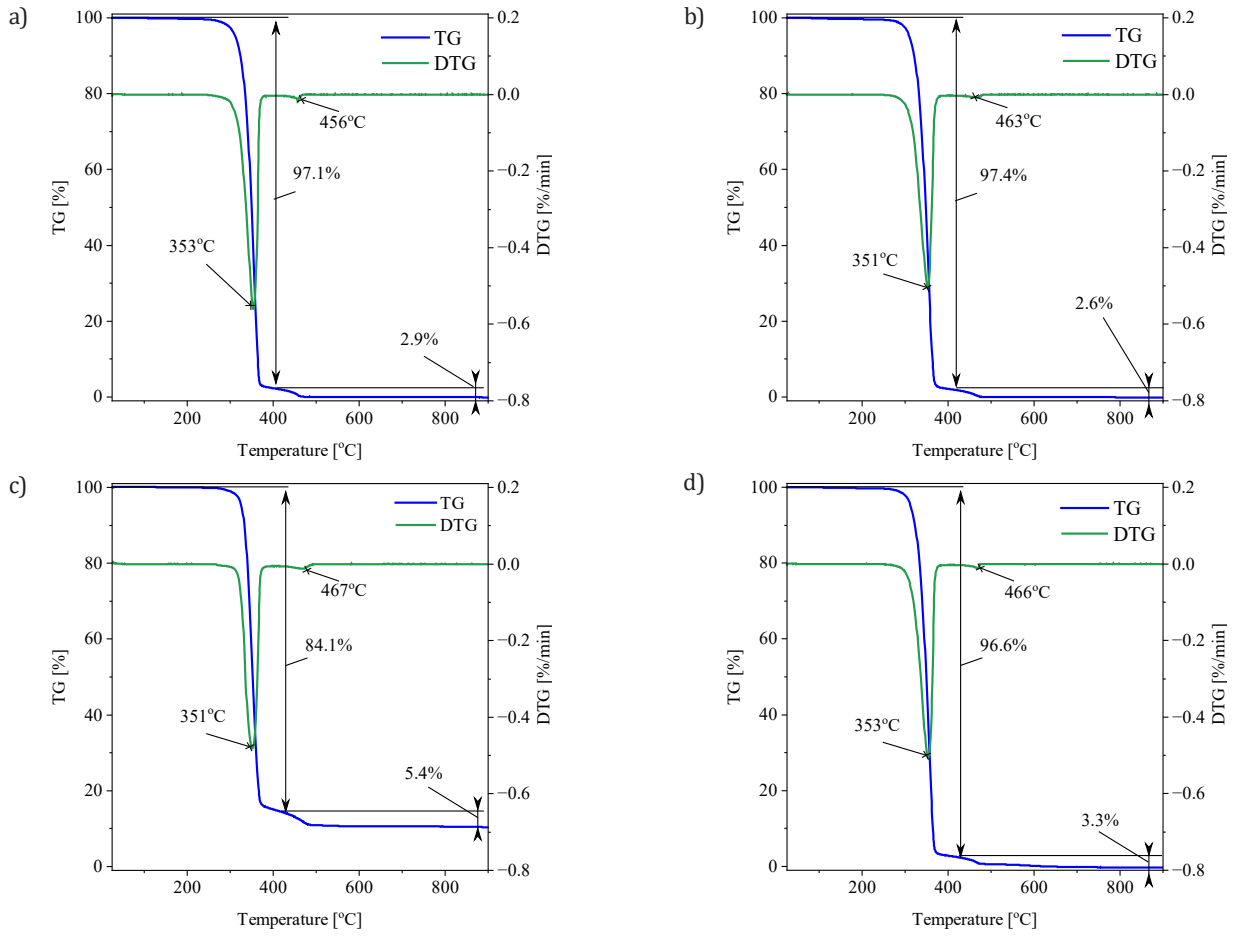

Fig. 1. TG-DTG curves of: a) PLA1; b) PLA7; c) ALFA+W; d) GRAFYLON®

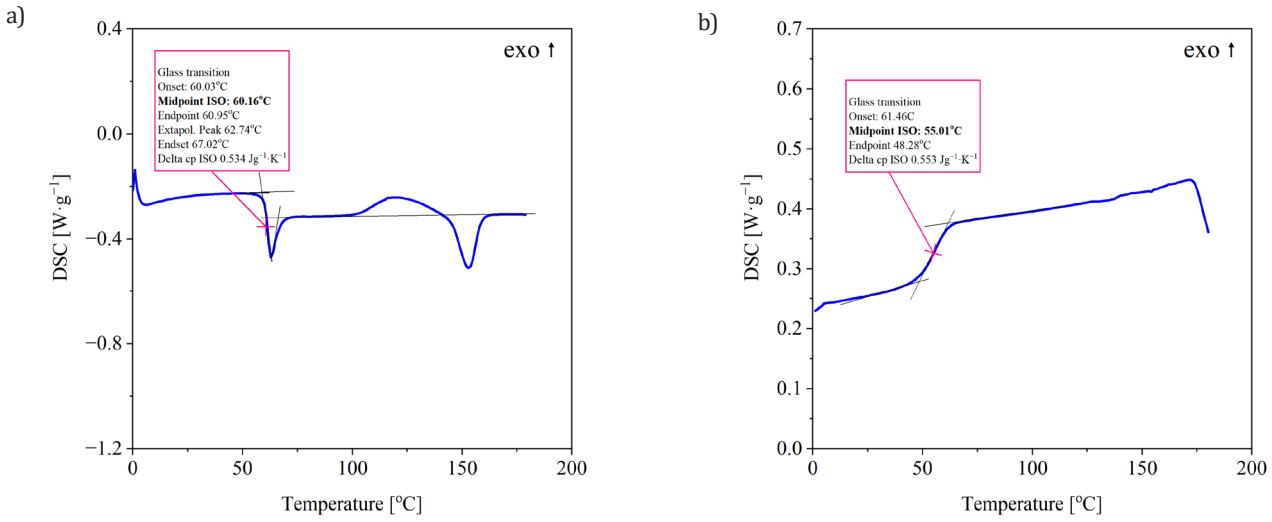

Fig. 2. DSC curves of PLA1: a) heating; b) cooling

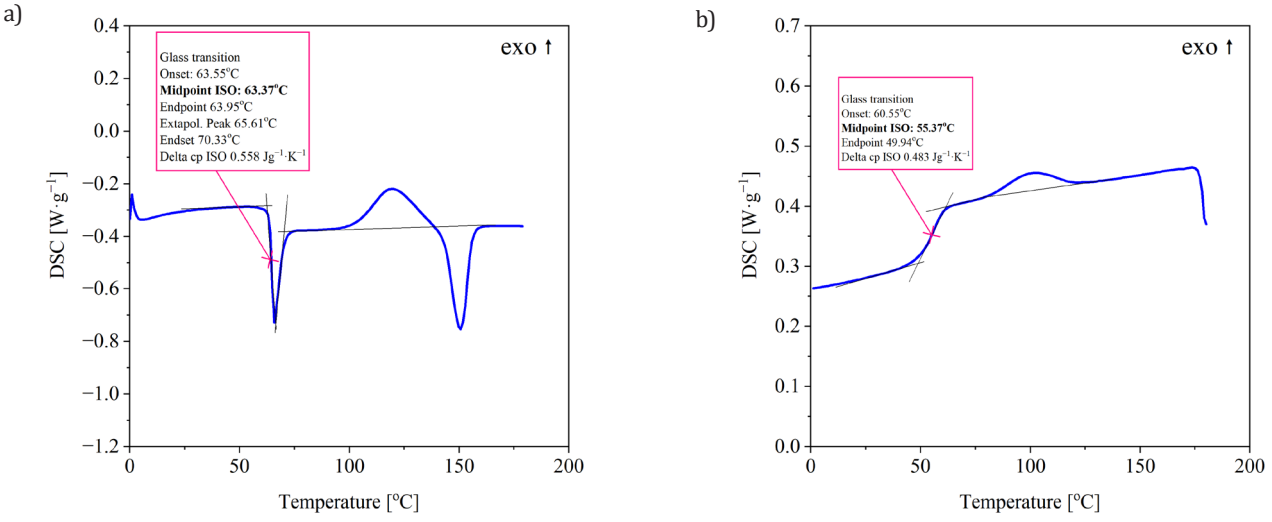

Fig. 3. DSC curves of PLA7: a) heating; b) cooling

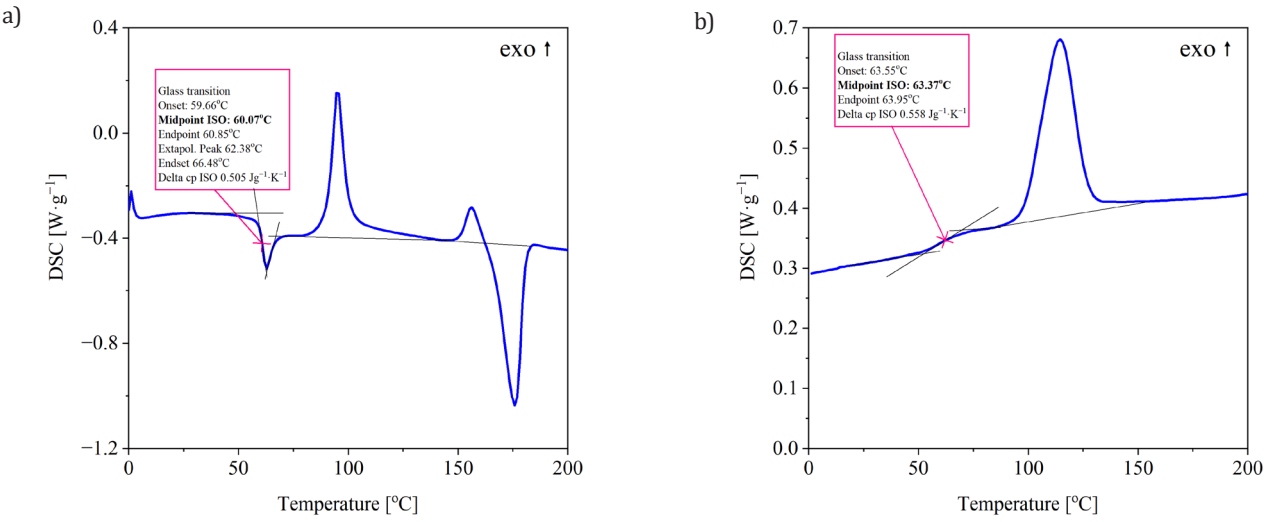

Fig. 4. DSC curves of ALFA+W: a) heating; b) cooling

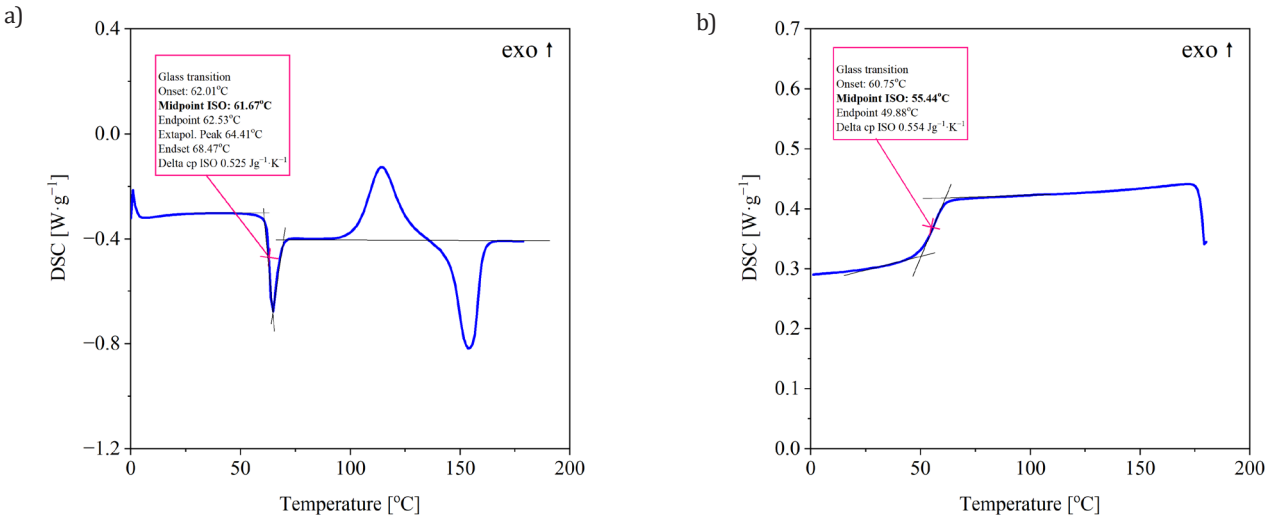

Fig. 5. DSC curves of GRAFYLON®: a) heating; b) cooling

Table 2
Glass transition and melting point temperature for PLA1, PLA7, ALFA+W and GRAFYLON®

Parameter	Sample			
	PLA1	PLA7	ALFA+W	GRAFYLON®
Extrapolated temperature of onset of glass transition ($T_{ei,g}$) [°C]	60.03	63.55	59.66	62.01
Extrapolated temperature end of glass transition ($T_{ef,g}$) [°C]	67.02	70.33	66.48	68.47
Glass transition temp. (T_g)[°C]	60.16	63.37	60.07	61.67
Extrapolated initial melting point temp. ($T_{ei,m}$) [°C]	144.91	142.94	165.89	144.76
Melting point temp. ($T_{p,m}$) [°C]	154.97	150.55	175.89	153.87

3.2. Structural analysis

DRIFT spectra for the samples were recorded in the temperature range of 20–500°C, indicating that with increasing temperature the shape as well as the position and intensity of particular bands changed. Some of them intensified and some of them disappeared completely, which indicates the progressive degradation of the polymer chain due to the temperature. New bands were also formed during the temperature increase, which was indicated in the sample structure. DRIFT spectra of PLA are shown in Figures 6–9.

Recorded spectra for three samples: PLA1, PLA7 and ALFA+W at 20°C, contained characteristic bands originating from the vibrations group of atoms found in the PLA structure (Table 3). It was also observed that the spectra contained additional bands throughout the range of wave numbers, whose vibrational energy was often close to the vibrational energy of the bonds of atoms present in PLA. These vibrations come from the introduced additives to the base material of polylactide i.e., dyes and graphene. For the GRAFYLON® sample, a significantly reduced intensity of the bands was found across the considered range of wave numbers. This is probably due to the fact that the sample contains a significant amount of graphene, for which the detection of the vibrational energy of individual bonds is not possible in the mid-infrared range. It was found that the characteristic bands did not change up to a temperature of around 360°C.

Above the temperature of 360°C on the spectra of the examined samples in the region of wavenumbers 4000–2800 cm^{-1} a slow decrease in the intensity of particular bands is observed, which indicates progressing degradation of the samples. It is noteworthy that at 500°C, in the region of 1700 cm^{-1} characteristic bands of carbonyl group (>=C=O) are present and even an increase in intenisty of this band is observed. Additionally, the bands below 1450 cm^{-1} characteristic for C-C vibrations did not disappear, it confirms that all of the samples under consediration have not yet completely decomposed. In the case of the GRAFYLON® sample, no band in the region of wavenumbers 3600–3700 cm^{-1} was observed. It proves a lack of a tendency for water adsorption on the surface. Based on the analysis of DRIFT spectra, it can be concluded that the least thermostable filament is PLA1 material, and the most stable is GRAFYLON®. The thermostability of PLA7 and ALFA+W samples, on the other hand, is similar and proves the validity of manufacturing felt using recycled materials.

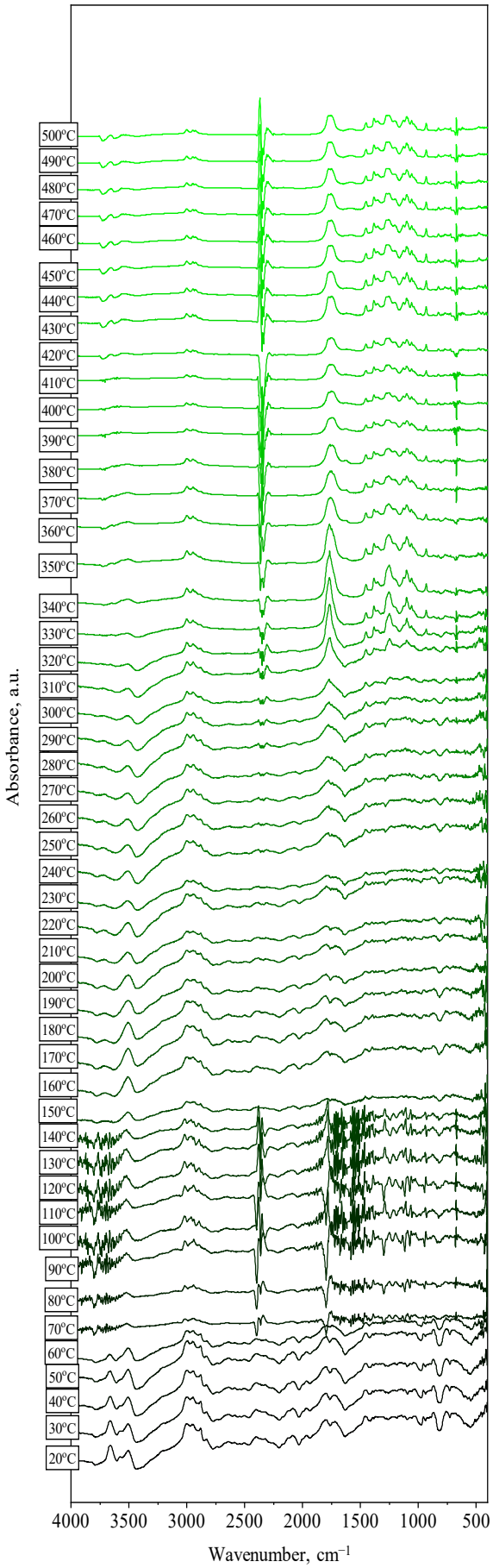

Fig. 6. DRIFT spectra of PLA1

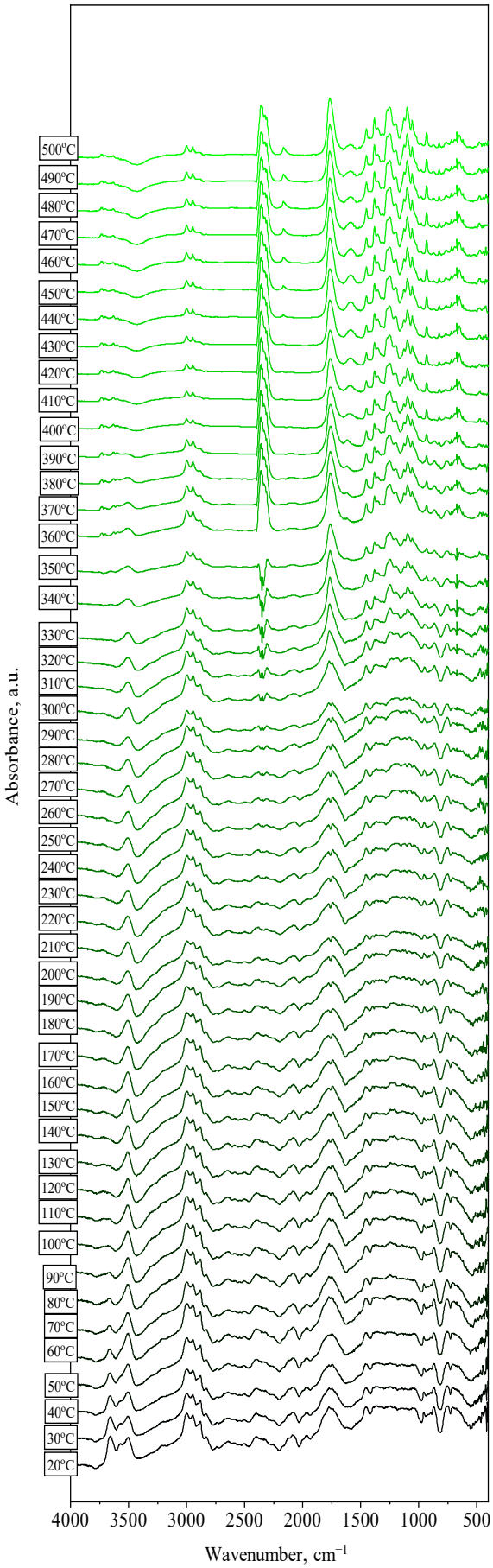

Fig. 7. DRIFT spectra of PLA7

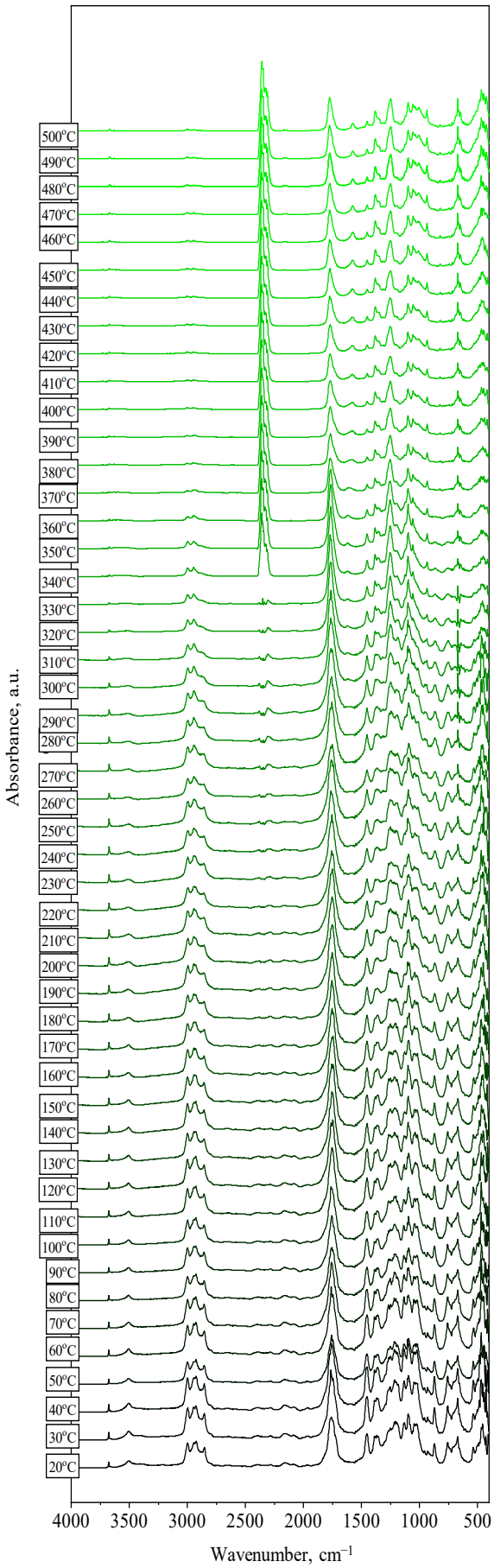

Fig. 8. DRIFT spectra of ALFA+W

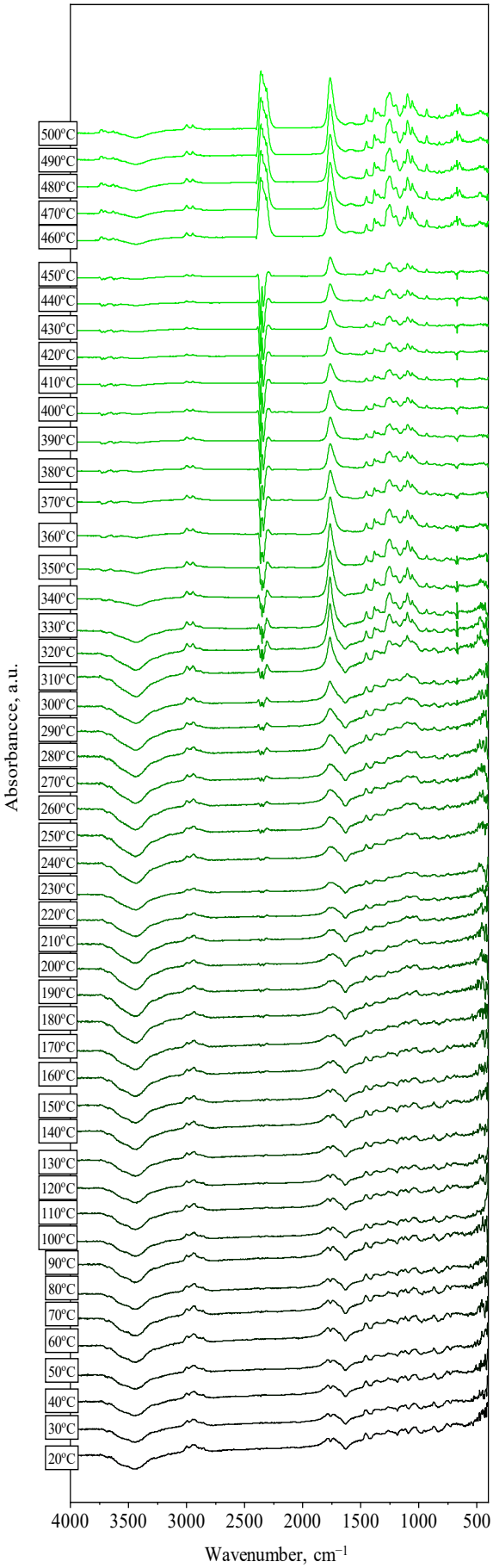

Fig. 9. DRIFT spectra of GRAFYLON®

Table 3
Characteristic absorption bands on the DRIFT spectra of PLA samples

Wavenumber [cm^{-1}]	Assignment	Remarks
3500–3400	*v*-OH	Band of free OH group (water adsorption)
2945–3000	*v*-C–H *v*(CH_2)	Stretching vibrations asymmetric and symmetric
1750–1760	v_s-C=O	Stretching vibrations of carbonyl group
1450–1455	β(CH_3)	In-plane bending vibrations
1380	δ-CH–	Deformation vibrations asymmetric and symmetric
1250–1220	–C=O	Bending vibrations
1170–1175	*v*-C–O–	Stretching vibrations
1030–1040	*v*-OH	Stretching vibrations
860–890	–C–C–	Stretching vibrations

4. CONCLUSIONS

Based on the thermal analysis of TG-DTG, it was confirmed that the degradation of the considered samples of PLA material begins around the temperature of 350°C. This fact indicates the possibility of their use in 3D printing processes. It has been shown that, among the tested samples, the material reinforced with graphene phase (GRAFYLON®) retains the best thermal properties, which results in even wider possibilities of its processing, including further modification, and wider usability for structural elements of vehicles with its participation. Moreover, the glass transition temperature for the supplied samples was determined by the DSC method. It was found that recycling and modification with graphene had no significant effect on the T_g value. The melting point and change to the melting enthalpy (ΔH_p) was also determined. The material from recyclate (ALFA+W) was characterized by a higher T_p value than the other samples by more than 20°C, hence it may be more suitable for use in the production of structural components operating at increased temperature. It has been shown that the most important structural changes under the influence of temperature begin above the temperature of 360°C. Conclusions from these studies find practical applications in determining the suitability of a given material for use in 3D printing technologies. It can be concluded that the tested materials exhibit adequate thermal stability for their use in the 3D printing process.

REFERENCES

[1] Siemiński P. & Budzik G. (2015). *Techniki przyrostowe. Druk 3D. Drukarki 3D.* Warszawa: Oficyna Wydawnicza Politechniki Warszawskiej.

[2] Ślusarczyk P. (2017). Nowa "krzywa hype'u Gartnera" dla sektora druku 3D. Retrieved from https://centrumdruku3d.pl/nowa-krzywa-hypeu-gartnera-dla-sektora-druku-3d/ [accessed 7.11.2022].

[3] Fontana L., Minetola P., Iuliano L., Rifuggiato S., Khandpur M.S. & Stiuso V. (2022). An investigation of the influence of 3D printing parameters on the tensile strength of PLA material. *Materials Today: Proceedings*, 57, 657–663. Doi: https://doi.org/10.1016/j.matpr.2022.02.078.

[4] Dodziuk H. (2019). *Druk 3D/AM. Zastosowania oraz skutki społeczne i gospodarcze*. Warszawa: Wydawnictwo Naukowe PWN.

[5] Notta-Cuvier D., Odent J., Delille R., Murariu M., Lauro F., Raquez J.M., Bennani B. & Dubois P. (2014). Tailoring polylactide (PLA) properties for automotive applications: Effect of addition of designed additives on main mechanical properties. *Polymer Testing*, 36(36), 1–9. Doi: https://doi.org/10.1016/j.polymertesting.2014.03.007.

[6] Jain R. & Gupta N. (2022). Design optimization of PLA lattice in 3D printing. *Materials Today: Proceedings*, 59, 1577–1583. Doi: https://doi.org/10.1016/j.matpr.2022.02.186.

[7] Grabowska B., Kaczmarska K., Cukrowicz S., Mączka E. & Bobrowski A. (2020). Polylactide used as filment in 3D printing – Part 1: FTIR, DRIFT and TG-DTG studies. *Journal of Casting & Materials Engineering*, 4(3), 48–52. Doi: https://doi.org/10.7494/jcme.2020.4.3.48.

[8] Przybytek A., Kucińska-Lipka J. & Janik H. (2016). Thermoplastic elastomer filaments and their application in 3D printing. *Elastomery*, 20(4), 32–39.

[9] Rabek J.F. (2012). *Polimery: otrzymywanie, metody badawcze, zastosowanie*. Warszawa: Wydawnictwo Naukowe PWN.

[10] Grabowska B. (2019). *Polimery. Budowa. Otrzymywanie. Właściwości. Aplikacje w odlewnictwie*. Kraków: Wydawnictwo Naukowe Akapit.

[11] Królikowski W. (2012). *Polimerowe kompozyty konstrukcyjne*. Warszawa: Wydawnictwo Naukowe PWN.

[12] Chanda M. & Roy S.K. (2019). *Industrial Polymers, Specialty Polymers, and Their Applications*. CRC PRESS.

[13] Integracja druku 3D w przemyśle motoryzacyjnym. (n.d.). Retrieved from https://hp3d.pl/blog/integracja-druku-3d-w-przemysle-motoryzacyjnym/ [accessed 7.11.2022].

[14] Szafrański B. (2017). Druk 3D w prototypowaniu i produkcji. *Główny Mechanik*, 5–6, 17–23.

[15] Filament ABS i PLA dla drukarek 3D. (n.d.). Retrieved from http://www.plastspaw.pl/filament-drukarki-3d.html [accessed 7.11.2022].

[16] PN-EN ISO 11358-1:2014-09: Tworzywa sztuczne – Termograwimetria (TG) polimerów – Część 1: Zasady ogólne. (2014). Retrieved from https://sklep.pkn.pl/pn-en-iso-11358-1-2014-09e.html.

[17] PN-EN ISO 11357-1:2016-11: Tworzywa sztuczne – Różnicowa kalorymetria skaningowa (DSC) – Część 1: Zasady ogólne. (2016). Retrieved from https://sklep.pkn.pl/pn-en-iso-11357-1-2016-11e.html.

[18] PN-EN ISO 11357-2:2020-09: Tworzywa sztuczne – Różnicowa kalorymetria skaningowa (DSC) – Część 2: Wyznaczanie temperatury zeszklenia i stopnia przejścia w stan szklisty. (2020). Retrieved from https://sklep.pkn.pl/pn-en-iso-11357-2-2020-09e.html.

[19] PN-EN ISO 11357-3:2018-06: Tworzywa sztuczne – Różnicowa kalorymetria skaningowa (DSC) - Część 3: Oznaczanie temperatury oraz entalpii topnienia i krystalizacji. (2018). Retrieved from https://sklep.pkn.pl/pn-en-iso-11357-3-2018-06e.html.

Journal of Casting & Materials Engineering Vol. 7 No. 4 (2023) 49–55
https://doi.org/10.7494/jcme.2023.7.4.49

The Circular Economy in Terms of Zinc Recovery from Industrial Waste – Directions for the Development and Profitability of Recycling

Artur Bobrowski*, Aleksander Nejranowski

AGH University of Krakow, Faculty of Foundry Engineering, Reymonta St. 23, 30-059 Krakow
e-mail: arturb@agh.edu.pl

Received: 28 March 2023 /Accepted: 22 November 2023/Published online: 15 December 2023.
This article is published with open access at AGH University of Science and Technology Journals.

Abstract

The article reviews the current state of the art in the field of zinc recycling. The results of model studies of the profitability (profitability) of the process of zinc recovery in precipitation in the form of dusts and sludges are presented. The cost of purchasing waste and the necessary energy and material expenditures were taken into account. It has been shown that access to a cheap source of waste is essential for the profitability of the zinc recovery process.

Keywords:

circular economy, industrial waste, recycling, zinc recovery, zinc dust, profitability of recycling process

1. INTRODUCTION

According to data [1, 2], the global annual production of zinc is over 13 million tons. Another source [3] states that the estimated global production of metallic zinc in 2007 was 11.4 million tons. Most of this, about 55% [4, 5], is used as a material for corrosion protection by galvanizing the surface. The remaining part is used for the production of alloys with other metals: brass and bronze alloys (about 20%), zinc alloys (13%) and other chemical materials (10%) [4]. Figure 1 shows the global consumption of zinc in various economic sectors.

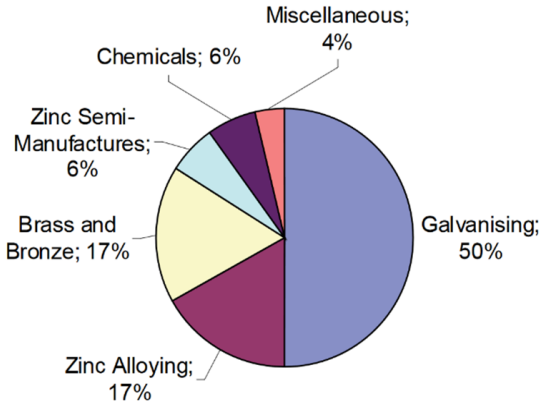

Fig. 1. Percentage share of zinc consumption depending on the sector of the economy, in the world perspective [5, 6]

The use of zinc as an anti-corrosion agent worldwide increased from 10.9 million tons in 2009 to 13.0 million tons in 2013 [5]. The authors [7] assume that at the current rate of consumption, the demand for zinc by 2050 will be 2.7 times higher than today. The main source of primary zinc are sulfide ores, containing from 2 to 30% of zinc, from which the so-called concentrates through the froth flotation process. Pure, metallic zinc is obtained via pyrometallurgical or hydrometallurgical processes [3, 8]. Figure 2 shows the technological operations of zinc production by hydrometallurgical and pyrometallurgical methods.

According to calculations, for the production of 1 kg of zinc from primary sources (from ore: copper, lead, zinc, silver, gold), which contains 62% of zinc, it is necessary to use resources that amount to the emission of 10.64 million tons of CO_2 per year or 0.03% of global CO_2 emissions [7]. In order to achieve climate goals, measures must be taken to reduce carbon dioxide emissions. One of the ways that can contribute to their achievement seems to be the secondary recovery of zinc from industrial waste – recycling. Thus, by meeting the main assumptions of the circular economy, the consumption of natural resources and environmental degradation are reduced, and at the same time the by-products generated in other areas of the economy are managed. In [9, 10], a sustainable circular economy is defined as a transformation in which the value of products, materials and resources is maintained in the economy for as long as possible, and the generation of waste is minimized [9, 11]. At the same time, efforts should be made to replace the linear economy, a diagram of which is shown in Figure 3, and to apply the assumptions of the circular economy as widely as possible (Fig. 4), bringing both environmental and economic benefits.

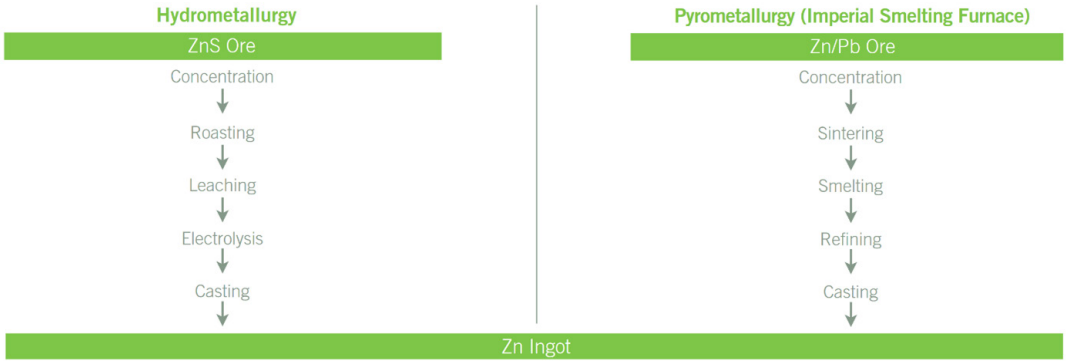

Fig. 2. Scheme of the hydrometallurgical and pyrometallurgical zinc production process [3]

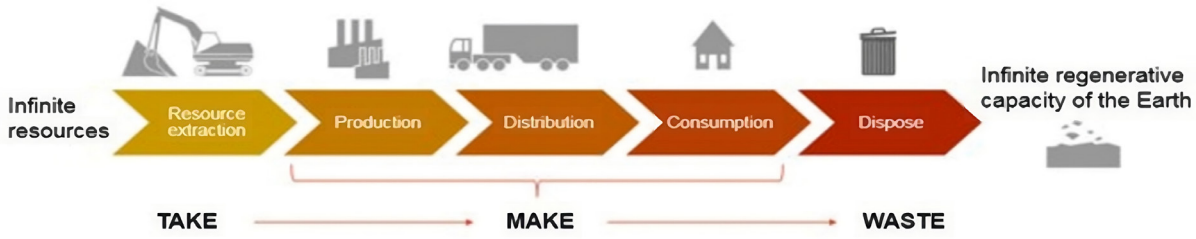

Fig. 3. Linear economy scheme [12]

Fig. 4. Diagram of the circular economy [13]

Some of the short and long term benefits of recycling and reusing mining and metal mining waste include [9, 11]:

- creation of financial assets,
- increasing resource efficiency by limiting the linear consumption of natural resources,
- limiting the production and collection of waste,
- encouraging innovation and development of local spin-offs,
- job creation,
- shared responsibility and ownership over the environment.

Zinc-containing waste is not only scrap such as castings. Significant amounts of zinc are found on anti-corrosive steel sheets that are recycled. During this process (smelting) the zinc evaporates and deposits in the form of dust on the filters. The current possibilities of recovering valuable raw materials and the desire to minimize the amount of waste make zinc-containing dusts and sludges a valuable source of this element and an alternative to obtaining it from primary sources. According to [14], in the European Union alone, in 2018, 74 Mt of crude steel was produced in electric arc

furnaces, at 2/3 of the total production capacity. Assuming the production of 17 kg/t of EAF steel per year, 1.26 Mt of EAF steel dust is generated, typically containing from 15% to 40% zinc. With a European recycling capacity of 1.1 Mt, most of the zinc in EAF dust is now recycled in the EU, while globally around 60% of EAF dust currently ends up in landfills. The dominant process used to smelt recycled materials with a high content of zinc is the Waelz rotary kiln, where the zinc is first reduced, then re-oxidized and recovered as impure zinc oxide containing 50–60% zinc [4]. A significant disadvantage of the pyrometallurgical method is the high energy demand, but also the need to use process gas purification systems. An additional problem of a technological nature are chloride and fluoride salts, which are characterized by a high corrosion potential. In turn, hydrometallurgical recycling methods allow for the processing of waste with a low content of zinc and are more environmentally friendly [8].

Figure 5 shows a comparison of energy consumption during individual zinc recovery processes by hydrometallurgy and pyrometallurgy, and Figure 6 shows the carbon footprint (carbon dioxide emission) per ton of zinc produced.

Based on data from Eurometaux (European non-ferrous metals association) and the Institute of Scrap Recycling Industries (ISRI), the energy demand for zinc recovery from waste and the associated carbon footprint were estimated (Table 1).

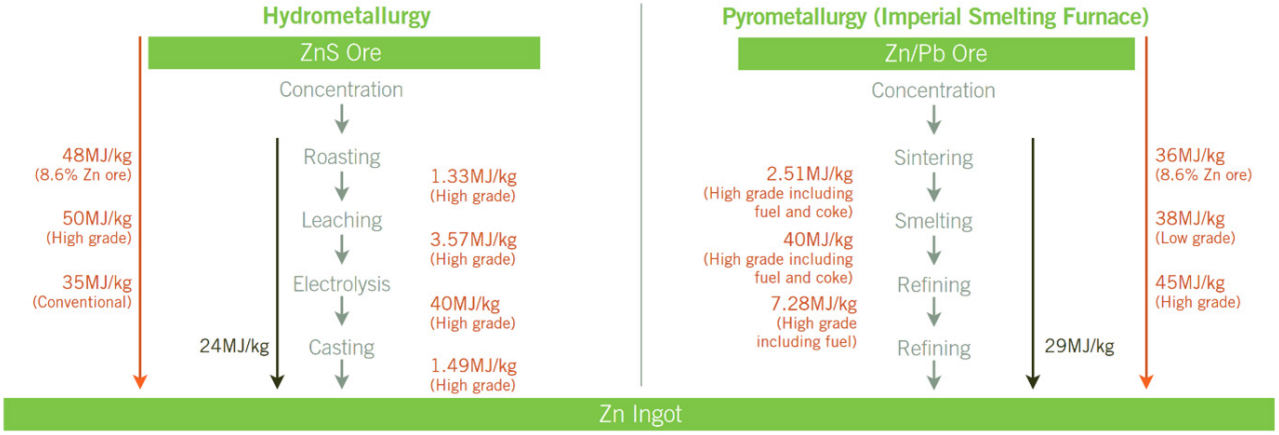

Fig. 5. Energy consumption in the process of zinc recovery by hydrometallurgy and pyrometallurgy [3]

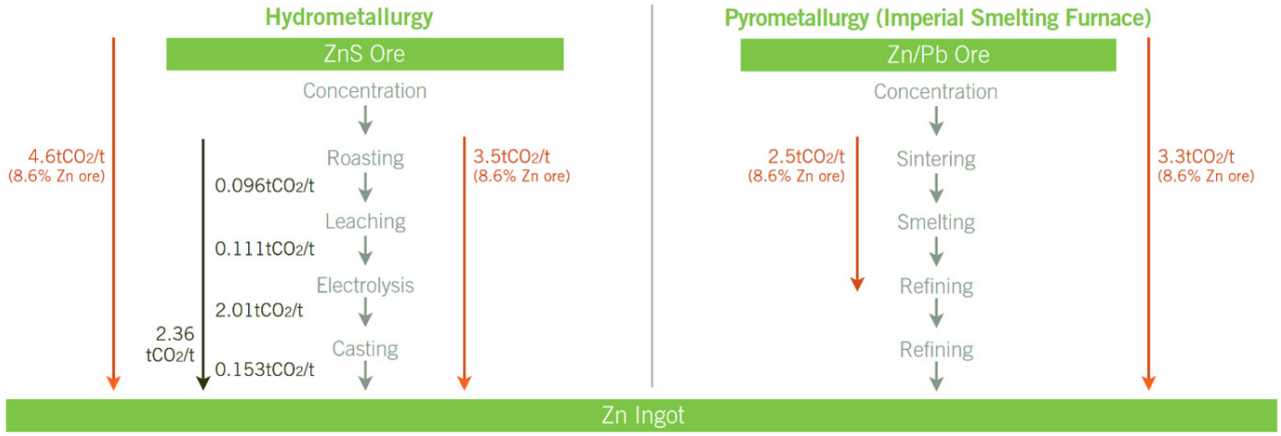

Fig. 6. Carbon footprint related to the hydrometallurgy and pyrometallurgy process [3]

Table 1
Energy demand for zinc recovery from waste (secondary metallurgy) and the associated carbon footprint. Own elaboration based on [3]

Process	Energy requirements			Carbon footprint [t CO_2/t Zn]
	energy requirement [MJ/kg Zn]	electricity [%]	additional	
Dezincing	54	–	–	4.6
Waelz-kiln process	18	93	1.2 t coke/t Zn	0.7–1.4
EZINEX	35	82	–	
DC-furnace	27	96	0.2 t coke/t Zn	

Table 2
Comparison of energy consumption (TJ)/100,000 tons for primary and secondary production of different types of metals [3]

Material	Primary	Secondary	Saving/100,000 tons
Aluminium	4700	240	4460
Copper	1690	630	1360
Ferrous	1400	1170	230
Lead	1000	13	987
Nickel	2064	186	1878
Tn	1820	20	1800
Zinc	2400	1800	600
Paper	3520	1880	1640

Table 3
Comparison of carbon footprint (100,00 t CO_2)/100,000 tons for the primary and secondary production of various types of metals [3]

Material	Primary	Secondary	Saving/100,000 tons
Aluminium	383	29	354
Copper	125	44	81
Ferrous	167	70	97
Lead	163	2	161
Nickel	212	22	190
Tn	218	3	215
Zinc	236	56	180
Paper	0.17	0.14	0.03

Tables 2 and 3, on the other hand, show that the zinc recycling process is both more economical, but also leaves a smaller carbon footprint compared to primary metallurgy. In terms of energy demand, the Waelz overburden process is particularly advantageous, but it requires the use of additional material in the form of coke, necessary for the reduction of zinc oxide. The report [3] clearly shows that per 100,000 tons of zinc, the energy demand for primary zinc production is 2400 TJ, and in the recycling process (secondary metallurgy) 1800 TJ, and the carbon footprint: 236,000 t CO_2 and 56,000 t CO_2, respectively.

Zinc-containing sludges are another source of zinc. At the ZGH "Bolesław" plant, they are subjected to a flotation process in order to obtain a Zn-Pb concentrate with an increased silver content. As a result of the sludge enrichment process, a Zn-Pb-Ag concentrate (and by-products) is obtained, which, after thickening, is sent for recovery in the Waelz overburden process, enabling the recovery of zinc and lead [15]. Currently, apart from the Waelz process, the Primus technique is used in Europe to recover zinc from dust with a higher content of zinc. In the case of waste containing smaller amounts of zinc, the DK, OxyCup and RedIron processes are used [5].

2. DESCRIPTION OF THE TECHNOLOGY USED TO ASSESS THE PROFITABILITY OF ZINC RECOVERY FROM DUST

The technology used for the tested model is based on the parallel processing of two zinc-containing waste materials, which are separated due to their chemical composition and semi-finished products (concentrates). The first group includes sludges from zinc hydrometallurgy, sludges from industrial wastewater treatment plants, sludges from acidic wastewater treatment plants and others. The second category of waste consists of steelmaking dusts generated during the melting of galvanized steel scrap in electric furnaces.

As a result of processing sludges containing approx. 12% zinc and 5% lead, a product is obtained in the form of granulated zinc concentrate with increased metal content, i.e. approx. 43–45% zinc and approx. 12–16% lead. As a result of the transformation of steelmaking dusts containing approx. 15–35% zinc and approx. 2–4% lead, a product is obtained in the form of a zinc concentrate with an increased content of metals up to approx. 65% zinc, in the case of lead approx. 4–6%. The process of waste processing and zinc recovery is carried out in rotary kilns. Their processing is a multi-stage process, which consists of a batch preparation stage, waste processing in rotary kilns (metallurgical process), a stage of processing the produced concentrate into the physical form required by the consumer, i.e. granulation of the zinc sludge obtained in the process of processing sludge from hydrometallurgy or the preparation of an aqueous suspension in the case of a concentrate obtained from the treatment of steelmaking dusts.

In the process of sludge processing, an additive regulating the so-called alkalinity module of the charge, which is quartz sand. In the case of processing dusts and sludges, it is necessary to introduce a reducer in the form of coke breeze or fine-grained anthracite. The consumption of the reducer is from 25% to 40% by weight compared to the dry weight of the zinc-bearing material. The materials prepared and mixed in this way are introduced into the working space of

the furnace. The movement of the charge is possible thanks to the appropriate inclination of the furnace and its rotational movement. The gases generated during the process move through the kiln in a counter-current to the charge, and their movement is possible thanks to the operation of the suction fan located behind the kiln. In the first stage, water is removed, and in the next stage, chemical compounds are decomposed.

Reduction of zinc oxide with coke breeze at high temperatures causes the zinc to evaporate and then re-oxidize. In the last zone of the furnace, slag is formed as a by-product of the process. At a temperature of 600–800°C, the slag leaves the furnace under the influence of gravity, and then, after being cooled with water, it is collected by a scraper conveyor and stored. Zinc oxide is captured in the devices of the cooling and dedusting installation, such as the dust chamber, exchange cooler, bag filter of intensive dedusting. Dusts from the bag filter contain the highest amount of zinc, with the least deposited in exchange coolers. Zinc concentrate is a product of the zinc filter dust process.

During the processing of steelmaking dusts, the zinc concentrate in the form of dust or water suspension is transported for further processing in the hydrometallurgical process. The zinc-lead concentrate extracted from the sludges is exposed to granulation in a drum granulator. The product of granulation is zinc-lead concentrate granulate, the subsequent processing of which enables the recovery of metallic zinc and lead – in a different pyrometallurgical process. Figure 7 shows the main reactions taking place in the Waelz collapse process.

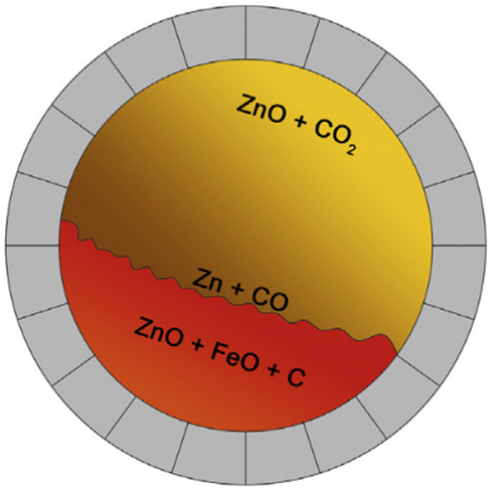

Reactions in gas phase (oxidizing)

$Zn + ½ O_2 \rightarrow ZnO$

$CO + ½ O_2 \rightarrow CO_2$

$Zn + CO + O_2 \rightarrow ZnO + CO_2$

Escaping CO gas and Zn vapor

Reactions in the charge (reducing)

$ZnO + CO \rightarrow Zn + CO_2$	$FeO + CO \rightarrow Fe + CO_2$
$CO_2 + C \rightarrow 2\ CO$	$CO_2 + C \rightarrow 2\ CO$
$ZnO + C \rightarrow Zn + CO$	$FeO + C \rightarrow Fe + CO$

Fig. 7. The main reactions taking place in the Waelz process [1]

3. MODEL PROFITABILITY ANALYSIS

The analysis of the profitability of zinc recovery processes from waste was carried out on the basis of a model prepared by ZGH „Bolesław" S.A., which is based on indicators determined on the basis of the average consumption of materials in a period of 12 months, reflecting the actual size of metallurgical waste processing. It was developed for the processing of 100,000 tons of waste. The analysis included the costs of:

- purchase of production materials:
  - dusts,
  - reducer,
  - limestone,
  - quartz sand,
  - $Ca(OH)_2$,
- gas,
- energy,
- compressed air,
- external services (waste management, equipment services, transport),
- taxes and fees (CO_2 emission fee, environmental fees, taxes and other fees),
- materials for repairs and repair services (conditions in which furnaces operate expose them to frequent repairs),
- remuneration for employees,
- health and safety services,
- depreciation of assets.

Table 4 summarizes the data on the percentage of zinc in zinc-bearing waste and the amount of zinc oxide produced from dusts and sludge, along with the percentage of zinc in the resulting product.

Table 5 shows the demand for materials necessary to carry out the waste recycling process, calculated on the basis of 100,000 tons.

Table 5 shows that the consumption of energy carriers for the processing of zinc-bearing dusts is higher than in the case of zinc-bearing sludges. This discrepancy is visible primarily in the demand for energy and limestone.

Table 6 shows the amount of slag generated in the recycling process, which is one of the by-products of the overburdening process.

Table 6 shows that for the adopted model, the processing of steelmaking dust generates over 4.5 times more slag than the processing of zinc-bearing sludge. With regard to the assumed model, Table 4 presents data on the percentage share of dusts and sludges purchased for the needs of the process. Taking into account the percentage share of materials in the overall waste processing, along with their origin (own resources, purchase from external companies, processing services), the revenue from the recovery process was calculated (Table 7).

The total revenue from the processing of zinc-bearing waste in the model under consideration consists primarily of the profit from the recovery of zinc from dusts, however, in order to ensure the continuity of the process and achieve the highest possible profitability, it is necessary to purchase them (an additional portion), which is a significant financial burden for the plant.

Table 4
Balance of the processing of dusts and zinc-bearing materials [16]

Type	Wet weight [t]	H_2O [%]	Dry weight [t]	Zn [%]	Zn content [t]
Dust (processing)	70,420.3	2.44	68,702.0	26.21	18,006.8
Sludges (processing)	29,579.7	31.04	20,398.2	16.28	3,320.8
Production ZnO from dusts*	27,493.0	0.00	27,493.0	61.42	16,886.2
Production ZnO from sludges**	7,736.0	8.40	7,086.2	44.05	3,121.5

* dusts yeld: 93.78%; **sludges yeld: 94.00%

Table 5
Consumption of materials, gas, compressed air and energy in the process of processing zinc-bearing dusts and sludges per 100,000 tons of waste [16]

Type	Material			Gas [m³]	Compressed air [m³]	Energy [kWh]
	reducer [t]	limestone [t]	*quartz sand [t]			
Zinc-bearing dusts	22,568.7	6,842.7	0	830,576.1	10,104,908.2	4,368,693.5
Zinc-bearing sludges	9,043.5	2,323.4	807.1	779,472.0	7,525,320.5	1,421,217.3
Total	31,612.2	9,166.1	807.1	1,610,048.1	17,630,228.7	5,789,910.8

Table 6
The amount of slag produced during the processing of zinc-bearing dusts and sludges [16]

Slag from dust processing [t]	58,070.3
Slag from sludge processing [t]	12,690.5
Total [t]	70,760.8

Table 7
Revenue from the zinc recovery process per 100,000 tons of waste [16]

Source of income	Amount [PLN]
Dust processing service	5,700,000
Sludge processing service	240,000
Dust purchase cost	4,800,000
Total	1,140,000

4. SUMMARY

With reference to the above-presented results of modeling the profitability of zinc recovery from waste in the sintering process, the following conclusions can be formulated:

- a significant cost that contributes to the final profitability of the overburdening process is the purchase of an additional amount of zinc-bearing dust. The adopted analysis, based on the adopted indicators, assumed the need to purchase 40% of dust to ensure the profitability of recycling.
- in addition to the fixed costs of the process of zinc recovery from waste, which includes, among others, purchase of materials, depreciation of assets, costs of energy, utilities, staff costs, ongoing repairs, the total profitability is also affected by:
  – zinc prices on the London Metal Exchange (LME),
  – exchange rates,
  – external services, e.g. waste management,
  – taxes and fees, i.e. CO_2 emissions fee, environmental fees.
- from the economic point of view, the most favorable factor for profitability is an increase in the price of zinc on the London Metal Exchange and an increase in the dollar exchange rate, with the lowest possible price of materials necessary for processing from waste suppliers,
- alternative sources of input materials with the highest possible zinc content should be sought.

REFERENCES

[1] Antrekowitsch J., Steinlechner S., Unger A., Rösler G., Pichler C. & Rumpold R. (2014). Zinc and Residue Recycling. In: Worrell E. & Reuter M.A. (Eds.), *Handbook of Recycling. State-of-the-art for Practitioners, Analysts, and Scientists*. Elsevier, 113–124. Doi: https://doi.org/10.1016/B978-0-12-396459-5.00009-X.
[2] World Bureau of Metal Statistics 2001–2011. Retrieved form https://www.lseg.com/en/data-analytics/trading-solutions/world-bureau-metal-statistics [accessed: 23.03.2023].
[3] Bureau of International Recycling (BIR) (2008). *Report on the Environmental Benefits of Recycling*. Retrieved from https://www.mgg-recycling.com/wp-content/uploads/2013/06/BIR_CO2_report.pdf [accessed: 23.03.2023].
[4] Wernick I.K. & Themelis N.J. (1998). Recycling metals for the environment. *Annual Review of Energy and the Environment*, (23), 465–497. Doi: https://doi.org/10.1146/annurev.energy.23.1.465.
[5] Stubbe G., Hillmann C. & Wolf C. (2016). Zinc and iron recovery from filter dust by melt bath injection into an induction furnace. *World of Metallurgy – Erzmetall*, 69(3), 161–168. Retrieved from https://www.velco.de/wp-content/uploads/2021/05/Erzmetall_Schmelzinjekt2016-1.pdf [accessed: 23.03.2023].
[6] International Lead and Zinc Study Group (ILZSG): Statistics 2014 (www.ilzsg.org).
[7] Ng K.S., Head I., Premier G.C., Scott K., Yu E., Lloyd J. & Sadhukhan J. (2016). A multilevel sustainability analysis of zinc recovery from wastes. *Resources, Conversion and Recycling* (113), 88–105. Doi: https://doi.org/10.1016/j.resconrec.2016.05.013.
[8] Jha M.K., Kumar V. & Singh R.J. (2001). Review of hydrometallurgical recovery of zinc from industrial wastes. *Resources, Conservation and Recycling*, 33(4), 1–22. Doi: https://doi.org/10.1016/S0921-3449(00)00095-1.

[9] Matinde E., Simate G.S. & Ndlovu S. (2018). Mining and metallurgical wastes: a review of recycling and re-use practices. *Journal of the Southern African Institute of Mining and Metallurgy*, 118, 825–844. Retrieved from https://www.researchgate.net/publication/324602638 [accessed: 23.03.2023].

[10] European Commission (2015). *Closing the Loop: An EU action plan for Circular Economy*. COM 614/2. European Commission, Brussels. Retrieved from http://eurlex.europa.eu/resource.html?uri=cellar:8a8ef5e8-99a0-11e5-b3b7-01aa75ed71a1.0012.02/DOC_1&format=PDF [accessed: 24.11.2017].

[11] Lottermoser B.G. (2011). Recycling, reuse and rehabilitation of mine wastes. *Elements*, (7)6, 405–410. Doi: https://doi.org/10.2113/gselements.7.6.405.

[12] Wautelet T. (2018). *Exploring the role of independent retailers in the circular economy: a case study approach* [Master of Business Administration]. European University for Economics and Management, Luxembourg.

[13] *Circular economy: definition, importance and benefits*. Retrieved from https://www.europarl.europa.eu/news/en/headlines/economy/20151201STO05603/circular-economy-definition-importance-and-benefits [accessed: 23.03.2023].

[14] Koukkari P., Riihimäki T. & Ollonqvist P.-P. (2022). New Hydrometallurgical Treatment to Recover Zinc and Iron from EAF Dust. *Word of Metallurgy – Erzmetall*, 75(1), 1–8.

[15] *Raport o bezpieczeństwie dla ZGH „Bolesław" S.A.* (2020). Retrieved from https://zghboleslaw.pl/images/pdf/2020/ZGHRoB-streszczenie21072020.pdf [accessed 23.03.2023].

[16] Nejranowski A. (2022). *Recykling pyłów i szlamów z procesów metalurgicznych w aspekcie technologicznym i ekonomicznym* [Engineering thesis]. AGH University of Krakow, Krakow.

Journal of Casting & Materials Engineering Vol. 7 No. 2 (2022) 56–62
https://doi.org/10.7494/jcme.2023.7.4.56

Effect of Titanium Alloying of Zn-Al-Cu Alloys for High Pressure Die Casting in Production Conditions

Łukasz Pasierb[a]*, Jan Łakomski[a], Krzysztof Figurski[b]

[a] Saga Poland, Guzowska 4, 96-515 Teresin, Poland
[b] Warsaw University of Technology, Institute of Manufacturing Technology, Narbutta St. 85, 02-524 Warsaw, Poland
**e-mail:* lpasierb@saga-mb.eu

Received: 29 November 2023 /Accepted: 14 December 2023 /Published online: 15 December 2023.
This article is published with open access at AGH University of Science and Technology Journals.

Abstract

The paper presents the possibility of the industrial production of Zn4Al3Cu alloy with the addition of 0.41% Ti. Tests are described on the manner of introducing the ZnTi2 master alloy to the alloy, so that the chemical composition of the desirable elements proportion is obtained. The chemical persistence of the Zn4Al3CuTi was determined as low in the conditions of the long heating of the alloy before casting. Tests on the microstructure and mechanical properties of the obtained alloys were also conducted. The strength of the die-cast Zn4Al3Cu alloy was 265 MPa and, when measured on samples taken from the high pressure die-cast, it reached 369 MPa. It was determined that the addition of titanium to the Zn4Al3Cu alloy causes significant refinement of the structure and contributes to the formation of intermetallic phases.

Keywords:

HPDC, zinc alloys, titanium additives, microstructure, mechanical properties

1. INTRODUCTION

Owing to their favourable casting and utility properties, foundry zinc alloys are employed in a wide range of applications. They demonstrate a relatively low melting temperature and, consequently, a low casting temperature and good castability. They are used particularly frequently in pressure casting. In zinc alloys, the main alloying additives are aluminium and copper, with small quantities of magnesium, manganese, iron, nickel, zirconium and titanium.

The addition of titanium to zinc alloys produced by pressure casting may have a varying degree of influence on the properties of the alloy. Titanium may introduce a change in the mechanical properties, such as increased tensile strength, hardness, wear resistance of the die-cast zinc alloy [1]. Titanium may also contribute to the reduction of the alloy's susceptibility to hot cracking during solidification, improving its castability and reducing faults in the final product [1–4]. Additives of titanium may increase strength at high temperatures and the stability of die-cast zinc alloy, ensuring that it is more suitable for applications where higher temperatures are the problem.

In zinc alloys, titanium may also act as grain refiner. Grain refinement involves adding some elements, often in small amounts, in order to facilitate the creation of finer and evenly spread grains in the alloy microstructure by heterogeneous nucleation. Titanium has a high preference to oxygen and easily forms titanium oxides. When titanium is added to the molten zinc alloy, those titanium oxides particles are the spots of heterogeneous nucleation. During the cooling process and solidification, these particles create spaces around which zinc solidifies. As solidification begins, multiple little grains compete for space, constraining the growth of other grains. Such competition additionally contributes to the formation of a fine-grained microstructure. Finer grains usually offer higher strength and increased wear resistance in comparison to larger ones. The effectiveness of titanium as a grain refiner may depend on various factors, including the concentration of titanium in an alloy, solidification speed, cooling rate, and the presence of other alloying elements. Proper control over those factors is essential for obtaining the desirable grain refinement effect. Additionally, the specific mechanism of grain refinement may differ depending on the alloy structure and interaction among titanium and other elements in the alloy. For example, in aluminium alloys, titanium forms certain intermetallic compounds that additionally serve as effective nucleation spots [2, 5–7]. Titanium additive to zinc alloys may be analysed with the use of the phase equilibrium systems. In pure zinc, at ambient temperatures, titanium solubility is negligible and amounts to

about 0.02% by weight (Fig. 1) [8]. At the eutectic point, at the temperature of 418.6°C, its maximum solubility is at the level of 0.2% by weight. The above condition means that the addition of titanium as an alloying element causes solid solution hardening and Zn-Ti intermetallic phases hardening. The increase of the alloying element concentration leads to the formation of primary precipitates which are increasingly richer in titanium.

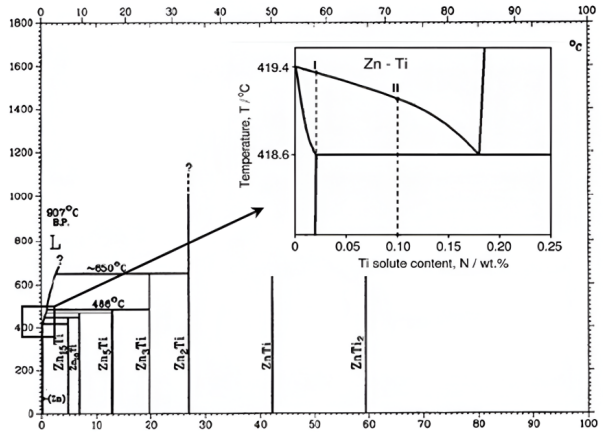

Fig. 1. Two-component Zn-Ti phase equilibrium system. The magnified part presents details of the zinc side [8]

Researchers have been interested in the Ti-Zn system for some years now, as Ti additives to Zn act as a grain refiner and they increase creep resistance in rolled alloys [9]. The solubility of Ti in Zn is estimated to be at 0.01% to 0.02% Ti at 300°C. It is assumed that the equilibrium phases are $Zn_{15}Ti$, $Zn_{10}Ti$, Zn_5Ti, Zn_3Ti, Zn_2Ti, ZnTi and $ZnTi_2$. $Zn_{15}Ti$ phase is the richest Zn compound.

Adding titanium to a zinc alloy which includes Al and Cu in its composition gives a similar effect but the number of additional intermetallic phases formed is significantly higher. Taking into consideration the analysis of tables, including the standardised chemical composition of zinc alloys, in the tests Zn4Al3Cu alloy modified by titanium was taken into account due to, i.a., specialised literature available, where cases of such a modification are described. For example, in [10], what was tested was the influence of a modification on the change in the degree of refinement of the structure of zinc alloys of an average aluminium content. Tests were conducted on Zn alloy – 10% by weight of Al (ZnAl10), modified before casting to sand mould by an additive of modifying master alloy Zn – 3.2% by weight of Ti (ZnTi3.2). It was determined that the effect of a significant microstructure refinement is visible when titanium is added in the amount of 25 ppm, 50 ppm and 100 ppm. Modification by adding more titanium, i.e. 200 ppm and 400 ppm, does not result in the further refinement of α-dendrites (Al). In the paper [1], it was proven that the titanium additive is beneficial to distribution, strength, hot crack strength, and tightness of a two-component Zn-Al alloy (48% Al). Titanium causes the formation of $TiAl_3$ particles that form nuclei of crystallisation. However, too many $TiAl_3$ particles may result in segregation in the alloys and may reduce the effect of grain refinement. An analysis of the literature demonstrated that there were no structure modification tests conducted in commercial (multi-component) zinc alloys.

To sum up, adding titanium to zinc alloys may entail challenges in applications, both in terms of structures and properties obtained, as well as technological obstacles. Titanium has a higher melting point than zinc, so the alloy smelting characteristics may change. What is more, achieving the even distribution of titanium in the entire alloy may be difficult, and proper processing techniques are required to ensure such an even distribution. Additionally, typical alloying elements added to zinc, i.e., Al and Cu, also change the structure, nature and properties of the alloy. Therefore, precise benefits and results of titanium additives depend on particular composition, conditions of processing and designed application of the zinc alloy for die casting. It is absolutely crucial to carry out precise tests and analyses in order to optimise the alloy composition and processing parameters, particularly for industrial conditions.

2. ASSESSMENT OF ALLOYING POSSIBILITIES OF ZINC ALLOY FOR DIE CASTING

In order to conduct the tests, it was decided to prepare an Zn4Al3CuTi alloy that requires the addition of titanium to the alloy nominally 4% by weight of aluminium and 3% by weight of copper. Commercially available preliminary alloy ZnTi2 (master alloy) includes up to 2% of titanium by weight. Master alloys with a higher content of titanium are impossible to encounter due to the rapidly growing liquidus curve along the increase in titanium concentration. If the target titanium concentration in Zn4Al3CuTi alloy is 0.2 by weight, it approximately corresponds to the eutectic point. In order to achieve this scope, per each 10 kg of Zn4Al3Cu alloy, 1 kg of ZnTi2 master alloy needs to be added. This means the significant dilution of other alloy constituents down to values below the lower limit admissible by the standard. Within the tests, a procedure of preparation of liquid Zn4Al3Cu alloy with titanium additive was devised. The procedure is described below.

In order to compensate the components, a commercially available AlCu50 master alloy was used, consisting of aluminium and copper in equal parts by weight. The liquidus temperature of this alloy is 600°C, and the solidus line at its lowest eutectic point is 545°C. This means that, in order to effectively dissolve AlCu50 master alloy, the alloy temperature should be increased over 550°C. Liquid material preparation time is crucial to ensure appropriate process productivity. The hot-chamber HPDC machine is the most expensive component of the system, and that is why its performance affects the viability of the entire casting process. The amount of the alloy prepared has to consider the ongoing continued parts production. To achieve minimal down-time of the HPDC machine, the assumption of creating a dedicated alloy mixing station was made. In terms to make the alloying procedure as fast as possible, the decision to use an induction furnace was conducted. Therefore, a special melting station was prepared, including the induction furnace with the specially made PLC-based controller equipped with thermocouples inserted directly into the furnace crucible, to allow a full control of an alloy temperature and minimalize the risk of burning out alloy components. Additionally, the induction heating technology offers the important advantage of the ability to mix the

material occasioned by magnetic field and convection in liquid, something which is especially useful in making modification of the alloy composition.

Tests during the pressure die casting of Zn4Al3CuTi alloys were conducted on a dedicated, specially made 8-cavity die. In each case, the casting cycle lasted for 20 s. The weight of castings with intake pass-through systems in the most demanding case achieved 700 g meaning that, with the assumed time of injection, there is a need to ensure 125 kg of material per hour of the casting machine's operations. With the induction furnace volume being efficiently 250 kg of alloy, alloying time of Zn4Al3CuTi could not exceed 2 h. The first tests conducted in line with the original procedure showed that preparation of one batch of alloy (from the input of feedstock to tapping of alloy) took about 5.5 h, what was not a satisfactory result. During the next tests, the alloying procedure was modified by changing the time of feeding the furnace. During the first optimisation, the base alloy was divided into two parts – the first one, about 80% by weight, for the initial alloying and subject to overheating, and the second one, about 20% of feedstock, to be added at the moment the dissolving of AlCu50 master alloy is over. This procedure results in a very rapid reduction of temperature from 550°C to the required level of 450°C, reducing the alloying time to about 4 h. The most time-consuming stage of the alloying procedure is the period of the overheating of the alloy and the dissolution of AlCu50 master alloy.

During the next technological tests, attempts were taken to obtain the alloy at a temperature not higher than 450°C. With the use of the casting machine furnace, tests of the rate of AlCu50 master alloy dissolution in 450°C were conducted. This time span may be shortened by using small fragments of the master alloy and the agitation of the alloy. During the tests, 2 cm × 2 cm × 4 cm pieces were used and an additional agitator operating at 0.5 r.p.s. was applied. The described conditions were: temperature of 450°C coupled with intense agitation enabled dissolution of added master alloy lumps within the time range of 2 h to 2.5 h. From the technological point of view, the time span is too long and it prevents the casting machine from operating in a continuous cycle. In order to accelerate the kinetics of the master alloy dissolution, its modification with the use of ZnTi2-AlCu50 alloy was proposed. Using an additional furnace, another pre-alloy was prepared, consisting of 50% by weight of ZnTi2 and 50% by weight of AlCu50. An exemplary photograph of the cast master alloy is presented in Figure 2.

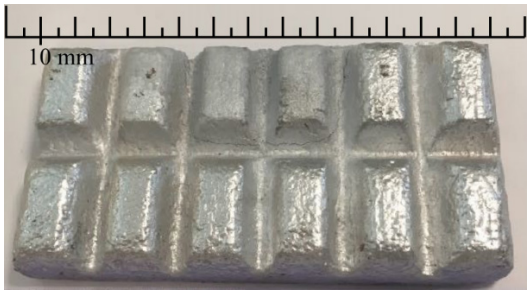

Fig. 2. Castings made of master alloy with chemical composition: 50% by weight of AlCu50 + 50% by weight of ZnTi2

Once again, the tests of alloying at the temperature of 450°C and with intense agitation began. The master alloy dissolved within the time not exceeding 10 min, what translates into tenfold acceleration of the process. The above experiments were repeated at the tests with the use of the dedicated induction furnace, during preparation of Zn4Al3CuTi alloy. ZnTi2-AlCu50 master alloy was added already at the stage of the first furnace feeding, which means that at the moment of achieving the correct temperature and readiness to tap – it was already dissolved. The condition of agitation was also met during melting in the induction furnace, where intense movement of the alloy was occasioned by magnetic field and convection in liquid.

Tests conducted with the modified AlCu50 master alloy showed a significant possibility to shorten the alloying time. It was achieved by the modification of the master alloy and the complete elimination of the overheating stage. This solution shortened the total time of the alloy preparation to about 2 h, increasing productivity and at the same time simplifying the entire procedure of the Zn4Al3CuTi alloy preparation. The achieved total alloying time is also sufficient for ensuring the continuous supply of liquid alloy to a hot chamber casting machine, and by this its uninterrupted operation. Continuity of the process is essential element of the high-pressure die casting technology that enables achieving high performance and repeatability of casting parameters. An important aspect is also the elimination of alloy overheating and the excessive oxidation such overheating entails.

3. CHEMICAL COMPOSITION TESTS

Experimental smeltings of base alloy – Zn4Al3Cu – with the addition of titanium, were carried out. In order to increase the hardness of the alloy, copper was introduced in a form of AlCu50 master alloy and titanium was introduced in a form of ZnTi2 master alloy, in various weight proportions. Tests on the chemical composition of the experimental smeltings were conducted with the use of a Solar M6 atomic absorption spectrophotometer, with the results presented in Table 1.

Table 1
Chemical composition of testing smeltings of Zn4Al3Cu and Zn4Al3CuTi alloys

Alloy	Al	Cu	Ti	Zn
Zn4Al3Cu	4.91	2.78	0.005	Re
Zn4Al3CuTi	4.28	2.77	0.410	Re

The analysis of chemical composition of the material was carried out. The material had the form of samples taken after a specified period of time from a pre-heating furnace where the alloy with Ti additives was prepared. The diagram in Figure 3 shows that over time the content of essential alloying elements diminishes [11]. Additional protection against the oxidation of the metal bath should be taken into consideration. A particularly adverse effect may be caused by the fluctuations in copper and titanium alloy, as those elements are responsible for hardness and the stabilisation of mechanical properties while soaking castings during possible subsequent technological operations, e.g. cataphoretic coating.

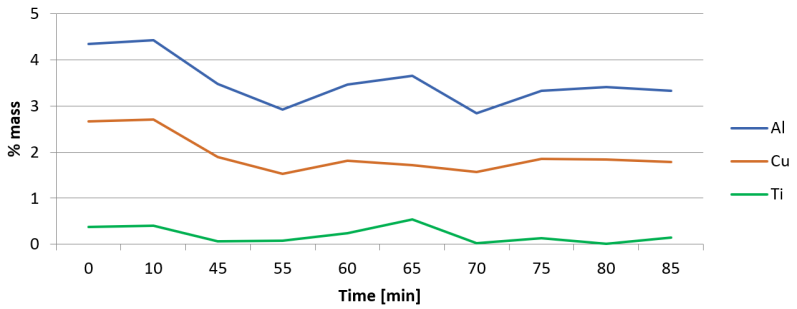

Fig. 3. Change in the content of selected elements in Zn4Al3Cu alloy over the time in a pre-heating furnace

4. MICROSTRUCTURE ANALYSIS

Tests of macrostructure, microstructure and phase composition were carried out on samples cut out of ingots of chemical composition of Zn4Al3Cu and of a pressure die-cast of Zn4Al3CuTi chemical composition. The tests were carried out with the use of a FEI Scios FEG high-resolution scanning electron microscope equipped with a thermal field-emission electron gun and with additional X-ray microanalysis system (EDS) and electron backscatter diffraction system (EBDS). At this stage of testing, none of the particular microstructure components were characterised. Only a significant influence of titanium as a structure refining element was determined. The microstructures obtained during the tests are shown in the Figure 4.

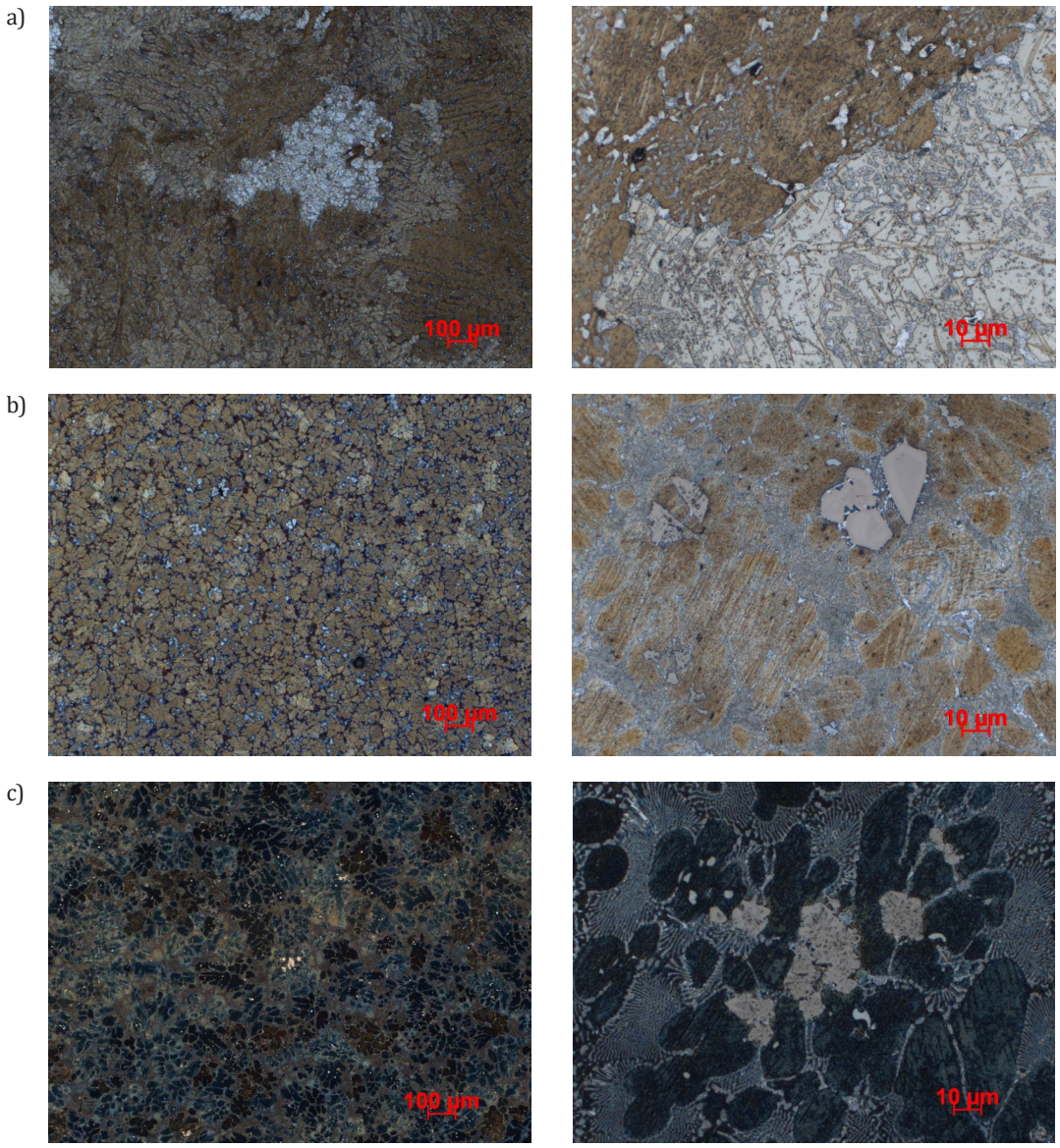

Fig. 4. Microstructures of testing castings: a) ingot surface; b) die-casting surface; c) high-pressure casting surface

The microstructure of the Zn4Al3Cu alloy includes dendrites of a solid solution based on zinc and eutectic based on zinc and aluminium (Fig. 5). It is a typical and distinctive microstructure of Zn-Al alloys. Due to its high cooling rate during casting, zinc is oversaturated into alloying additive for copper, which, by the mechanism of solid-solution hardening, significantly increases the mechanical parameters of the alloy. The titanium additive caused the formation of additional intermetallic phases. Their detailed description may be found in the publication [12]. Typically, already in a liquid form at the casting temperature of 450°C, an intermetallic phase forms, here denoted with the symbol T (Fig. 6). Its chemical composition may vary and may reach a wide range of various concentrations of zinc, aluminium, and titanium. Three-component phase T positions itself outside the eutectic or at the grain boundaries. T phase at the grain boundaries may inhibit growth of the primary phase η. Therefore, adding Ti to the zinc alloys may reduce the volume of the primary phase η. With Ti content in the Zn alloy above 0.05% by weight, coarse-grained phase T causes a decrease in the mechanical properties of the alloy [13].

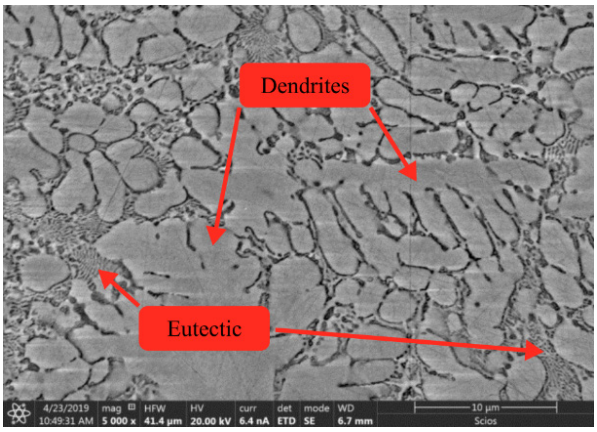

Fig. 5. Microstructure of Zn4Al3Cu alloy observed with the use of a scanning electron microscope with a BSE (back scattered electrons) detector

	% weight	% atomic
AlK	17.6	32.5
TiK	16.5	17.1
ZnK	66.0	50.4

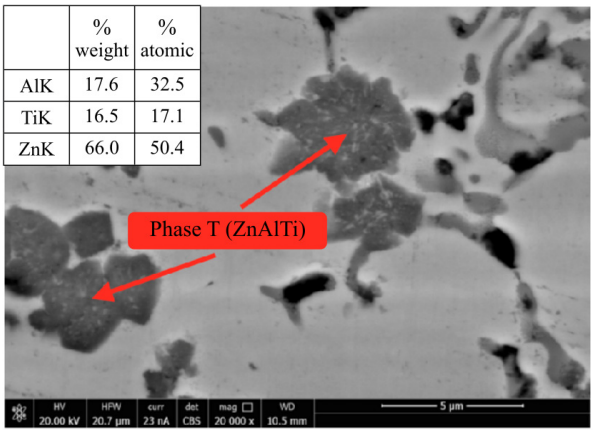

Fig. 6. Microstructure of Zn4Al3CuTi alloy observed with the use of a scanning electron microscope with back scattered electrons BSE detector

During the analysis, intermetallic phase based on iron was additionally identified. It is the result of contaminants coming mainly from the steel lining of the casting machine furnace.

The following structural components were defined:

- dendrites of zinc-based solid solution containing copper and aluminium,
- eutectic Al-Zn,
- phase T – ZnAlTi intermetallic phase,
- $Al_{13}Fe_4$ intermetallic phase.

5. TESTING OF MECHANICAL PROPERTIES

Statistical tensile tests were conducted in compliance with the PN-EN 10002-1 standard. The shape and dimensions of the samples are presented in Figure 7.

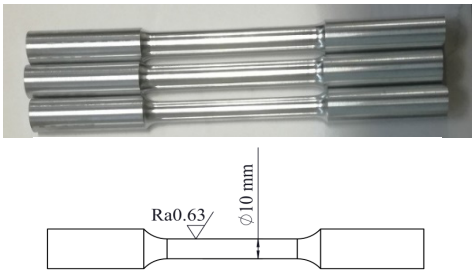

Fig. 7. Shape and dimensions of the samples for tensile strength tests

The details cast in the new technology were subjected to a series of mechanical tests. At first, the tests with the samples cast in semi-industrial conditions in a steel ingot mould were conducted. The alloy was prepared in a resistance furnace with mechanical agitation. In order to dissolve the AlCu50 master alloy, overheating of the alloy up to 550°C was employed. The final titanium content in the alloy was 0.41% by weight. The endurance of the die-cast Zn4Al3Cu alloy was 265 ±29 MPa and yield strength of 250 ±15 MPa. Significant spreads in the results and different natures of the stress-strain curves are caused by high porosity of castings made by gravity die casting. High-pressure casting is characterised by significantly different conditions of the alloy crystallisation, in effect giving completely different mechanical parameters of the finished detail. Moreover, the casts made in the discussed technology are usually thin-walled, something which is favourable for the better removal of heat, quicker crystallisation, and, in effect, refinement of the alloy microstructure. We should, therefore, expect considerably better strength parameters. The resulting cast has a complex shape with walls of various thickness in its cross-section. As the test shows, the porosity is mainly positioned in the central part of the material (Fig. 8). The additional problem during the tests concerned a small size of the discussed detail, giving little freedom when preparing the sample for the mechanical tests.

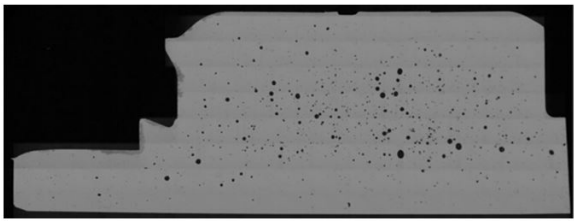

Fig. 8. Macro photographs of cross-section of the Zn4Al3CuTi alloy details

A method for cutting out the samples for tensile strength tests was suggested, i.e. cutting out of a material piece of thickness corresponding to half of the thickness of the cast detail. Thus, the influence of the spot of the collection of the sample (surface, centre of the cast) on material strength was determined. Exemplary samples for tests are presented in Figure 9. For the purpose of comparison, a photograph of the 33.5 mm-diameter detail is also attached. All the tests were conducted on Zn4Al3CuTi alloy of titanium content of 0.41% by weight. The discussed tests were carried out with the samples collected from the stabilised part of the casting process, i.e. after the thirtieth injection (smelting without alloy overheating).

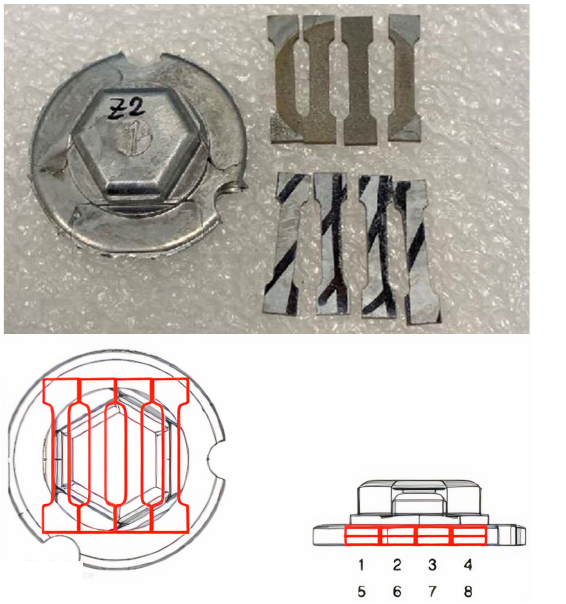

Fig. 9. Pattern of cutting out the samples for mechanical tests and photographs of those samples

The results of the tensile strength tests are given in Figure 10, comparing endurance qualities of the material taken from the surface and from the area closer to the details centre. Additionally, in the table attached to the figure, average values of yield strength, tensile strength, and total strain are presented. The best mechanical parameters were obtained on the samples cut out from the flat external part of the casting (samples 5, 6, 7, 8 – Fig. 9). Average yield strength $R_{0.2}$ and tensile strength R_m amounted to approx. 320 MPa and 370 MPa, respectively. Samples taken from the central part of the casting had slightly lower mechanical parameters, namely: $R_{0.2}$ = 270 MPa and R_m = 330 MPa, and substantially worse plasticity. Lower endurance was the effect of higher porosity in the casting centre, but also of the conditions for slower crystallisation during the casting process. Differences in the porosity were already visually apparent at the moment of comparing the two sets of samples. The results clearly show significantly higher tensile strength and pre-arranged yield strength for both the samples cut of the centre and those cut out from the casting surface, in comparison to the properties of the die-cast casting samples. Even in the worst case, the tested material has better strength than the material cast by gravity casting, which could be also found in other alloys used in high pressure casting techniques [14].

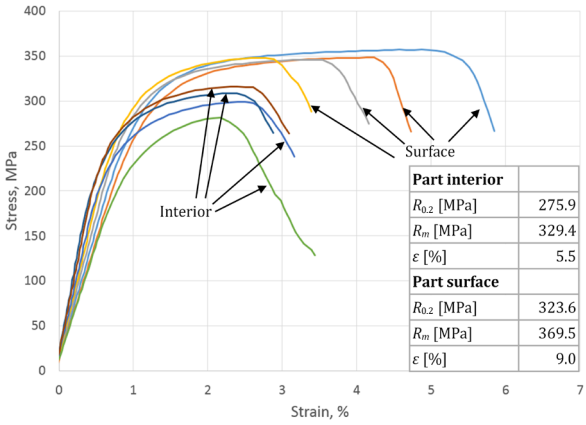

Fig. 10. Juxtaposition of tensile test curves for samples taken from the surface and from the centre of the detail

6. CONCLUSIONS

Based on the tests and analyses conducted, it was determined that:

1. The alloying procedure for Zn4Al3Cu alloy containing up to 0.41% of titanium in the form of die-casts and high-pressure castings was developed and tested in manufacturing conditions.
2. The chemical composition of an alloy demonstrating mechanical properties that exceed the properties identified for die-cast Zn4Al3Cu alloy was proposed.
3. Significant refinement of grain by means of the addition of 0.41% of titanium to the Zn4Al3Cu alloy cast by gravity casting was determined, as well as by high-pressure casting to a metal mould.
4. A change in chemical composition during the smelting process of the test alloy, Zn4Al3CuTi, was determined, requiring adjustments in the content of particular elements during the period when the metal is held in the melting furnace.

Acknowledgements

The presented results of R&D works were obtained by SAGA Poland sp. z o.o. as a result of the project called "Development and implementation of a production programme for auto glazing positioners equipment along with palletising process automation based on an innovative zinc alloy of improved thermal and mechanical resistance parameters" co-financed by the ERDF under the measure 1.2. SGOP 2014-2020 "Sectoral R&D programmes" agreement no. POIR.01.02.00-00-0229/16.

REFERENCES

[1] Yan Shu-qing, Xie Jing-pei Wang Wen-yan & Li Ji-wen (2009). Microstructure and tensile property of Zn-Al alloy reinforced with titanium produced by electrolysis. *Advanced Materials Research*, 79–82, 1415–1418. Doi: https://doi.org/10.4028/www.scientific.net/AMR.79-82.1415.

[2] Wang Jianhua, Wang Xiande, Tu Hao & Su Xuping (2011). Effects of titanium on microstructure and mechanical properties of ZnAl4Y alloy. *China Foundry*, 4, 397–400.

[3] *Engineering in Zinc, Today's Answer* (2019). Retrieved from https://www.zinc.org/engineering-in-zinc-todays-answer/ [accessed: 14.12.2023].

[4] Jemielewski J. (1970). *Odlewnictwo metali nieżelaznych*. Wydawnictwa Naukowo-Techniczne, Warszawa.
[5] Zyska A., Konopka Z., Łągiewka M., Nadolski M. & Chojnacki A. (2009). High-aluminium zinc alloy (ZnAl27Cu2) modified with titanium and boron. *Archives of Foundry Engineering*, 9(4), 237–240.
[6] Krajewski W. (1996). Phases of heterogeneous nucleation in the ZnAl25 alloy modified by ZnTi and AlTi master alloys. *Materials Research and Advanced Techniques*, 87(8), 645651.
[7] Leis-Speaker W. & Kallien L. (2013). Ageing and creep behaviour of Zinc-Diecasting-Alloys. International Zinc Diecasting Conference "Tradition & Innovation", Prague, Czech Republic, 13–14 June 2013. Retrieved from https://www.yumpu.com/en/document/view/40575985/ageing-and-creep-behaviour-of-zinc-diecasting-alloys-international- [accessed: 14.12.2023].
[8] Von W. Heine & U. Zwicker (1962). Untersuchungen an Legierungen des Systems Zink-Titan. *International Journal of Materials Research*, *Zeitschrift für Metallkunde*, 53(6), 380–385. Doi: https://doi.org/10.1515/ijmr-1962-530607.
[9] Sailin Fan, Changjun Wu, Ya Liu, Hao Tu, Xuping Su & Jianhua Wang (2017). 600 and 450°C isothermal sections of the Zn-Ce-Ti system. *Journal of Alloys and Compounds*, 709, 842–849. Doi: https://doi.org/10.1016/j.jallcom.2017.03.215.
[10] Piwowarski G., Buraś J. & Krajewski W.K. (2013). Wpływ zabiegu modyfikowania zaprawą ZnTi3,2 na mikrostrukturę stopu ZnAl10. *Archives of Foundry Engineering,* 13(spec. iss. 3), 129–132.
[11] Kallien L.H. & Leis W. (2011). Ageing of Zink Alloys. *International Foundry Research*, 64(1), 1–23.
[12] Sui Yang, Xuping Su, Jianhua Wang, Fucheng Yin, Zhi Li, Hao Tu & Haoping Peng (2010). The Zn-rich corner of the Zn-Al-Ti system at 723 K. *Journal of Alloys and Compounds*, 499(2), 194–199. Doi: https://doi.org/10.1016/j.jallcom.2010.03.148.
[13] Krupińska B., Rdzawski Z. & Labisz K. (2011). Crystallisation kinetics of the Zn-Al alloys modified with lanthanum and cerium. *Journal of Achievements of Materials and Manufacturing Engineering*, 46(2), 154–160.
[14] Pastirčák R., Brůna M., Matejka M. & Bolibruchová D. (2023). Effect of input parameters on the structure and properties of castings obtained via crystallization under pressure. *Metals*, 13(8), 1424. Doi: https://doi.org/10.3390/met13081424.